SRI International

Final Report • September 1991
Covering the Period 1 October 1987 through 30 September 1991

STUDIES OF SPATIAL INHOMOGENEITIES IN SMOKE PLUMES

F.L. Ludwig, Principal Scientist
Geoscience and Engineering Center

SRI Project 4427

Prepared for:

U.S. Army Research Office
Post Office Box 12211
Research Triangle Park, North Carolina 27709-2211
(Attention: Dr. Walter Bach)

Contract DAAL03-87-K-0143

333 Ravenswood Avenue • Menlo Park, CA 94025-3493 • (415) 326-6200 • FAX: (415) 326-5512 • Telex: 334486

REPORT DOCUMENTATION PAGE

Form Approved
OMB No. 0704-0188

1. AGENCY USE ONLY *(Leave Blank)*	2. REPORT DATE	3. REPORT TYPE AND DATES COVERED
	September 1991	Final Report, 1 Oct 1987—30 Jun 1991

4. TITLE AND SUBTITLE
Studies of Spatial Inhomogeneities in Smoke Plumes

5. FUNDING NUMBERS
DAAL03-87-K-0143

6. AUTHOR(S)
F.L. Ludwig

7. PERFORMING ORGANIZATION NAME(S) AND ADDRESS(ES)
SRI International
333 Ravenswood Avenue
Menlo Park, CA 94025

8. PERFORMING ORGANIZATION REPORT NUMBER
Final Report,
SRI Project 4427

9. SPONSORING/MONITORING AGENCY NAME(S) AND ADDRESS(ES)
U.S. Army Research Office
Post Office Box 12211
Research Triangle Park, North Carolina 27709-2211

10. SPONSORING/MONITORING AGENCY REPORT NUMBER
ARO 24881.3-GS

11. SUPPLEMENTARY NOTES
The view, opinions, and/or findings contained in this report are those of the author and should not be construed as an official Department of the Army position, policy, or decision, unless so designated by other documentation.

12a. DISTRIBUTION/AVAILABILITY STATEMENT
Approved for public release; distribution unlimited

12b. DISTRIBUTION CODE

13. ABSTRACT *(Maximum 200 words)*

Fractal concepts and their relevance to atmospheric processes are reviewed. Among these concepts are approaches to the estimation of fractal dimension based on the slope of the power spectrum, box counting and multidimensional feature analysis. These three approaches were applied to synthesized Brownian fractals, lidar cross sections of an elevated smoke plume, and infrared transmittance imagery of a ground-level smoke plume. The methodologies provided very good estimates of the known fractal dimensions of the sythesized data, but measures of the smoke plume characteristics exhibit considerable scatter. Extensions of the multiresolution feature analysis technique to vector fields, the use of empirically defined features is discussed. An example of an empirically defined vector feature is presented.

14. SUBJECT TERMS	15. NUMBER OF PAGES
Fractals, smoke plumes, atmospheric inhomogenieties	69
	16. PRICE CODE

17. SECURITY CLASSIFICATION OF REPORT	18. SECURITY CLASSIFICATION OF THIS PAGE	19. SECURITY CLASSIFICATION OF ABSTRACT	20. LIMITATION OF ABSTRACT
Unclassified	Unclassified	Unclassified	UL

CONTENTS

ILLUSTRATIONS

I INTRODUCTION

A. STATEMENT OF THE PROBLEM

The Army has a need for information about the distribution of smokes and chemical agents in the atmosphere, and their changes with time. With the increasing use of laser-guided weaponry and detection systems, there is a great need for quantitative measures of the probability that a clear line-of-sight will be found through an obscurant cloud. Chemical and biological defense planning also needs information about the likelihood that critical concentrations will be exceeded. This is the problem addressed by the research reported here.

Practical treatments of the smokes and gasses in the atmosphere have largely been limited to dealing with "average" or "most probable" results, i.e., smooth distributions. Any observation of atmospheric plumes suggests that such a picture does not accurately portray conditions at a single moment in time. Considerable structure and numerous inhomogeneities are usual features of such instantaneous plumes. This is not important for some applications, but in many instances it is, (e.g., when we wish to know the likelihood of being able to see through a plume, or of encountering short-term concentrations above some critical threshold).

There is reason to believe that the inhomogeneities in smoke plumes are "fractals." Some of these reasons are reviewed later. In the work reported here, I have identified suitable fractal analysis techniques and observations, and adapted and applied those techniques to the observations. Some of the techniques and results suggest that, in the future, they will lead to a much better understanding of atmospheric turbulent processes.

B. EVOLUTION OF THE RESEARCH APPROACH

Before proceeding to review why fractal concepts are important to the description of the inhomogeneous distributions of kinematic properties and the mixing of materials, I will briefly describe the evolution of the approach that was taken.

This work started with the intention of developing and applying methods for calculating the fractal dimension of atmospheric fields. As the project proceeded, it became apparent that fractal dimension provided only limited information and that the techniques used to estimate fractal dimension generated much valuable information that was discarded. For example:

- Simple box-counting methods do not use the spatial relationships between boxes containing members of the set at different scales.
- The Fourier methods do not use the distributions of amplitudes in the Fourier plane to infer anything about changes in anisotropy with scale.

Other factors were also troublesome. First, all the methods dealt only with the distribution of scalars in space, or with the distribution of members of some specified set (e.g., scalars with

values in a specified range). Another problem area was that fractal dimension was of rather limited use. Finally, there didn't seem to be much connection to the physics of the processes being studied, although there appeared to be some good reasons to think that fractals would be inherent to many atmospheric processes (e.g., the space fillingness of turbulence and the cascade of energy to ever smaller vortices).

At about this point J.G. Jones sent a preprint of the paper, "Multi-Resolution Analysis of Remotely-Sensed Data." This paper (eventually published—Jones et al., 1991) described how to use defined structures in a two-dimensional scalar field as the sets from which fractal dimension was calculated. Although still limited to scalars and two dimensions, it was clear that the technique could readily be extended to three dimensions. Furthermore, it soon became obvious that extension of the approach to two- and three-dimensional vector fields was also possible. This multiresolution feature analysis and other techniques are described in Section II.

With this new approach, it was theoretically possible to select "physically significant features," and use them in the analyses to learn more about the processes. It also appears that use of such features might significantly improve the realism of simulated inhomogeneous distributions. Of course, we must be able to define "significant features," the obvious line of reasoning is to devise a method whereby the data themselves would determine what was important. Statisticians frequently use principal component analysis for this purpose, and Lorenz (1956) had successfully used a closely related approach to define patterns of pressure and temperature variability for statistical weather forecasting. Lorenz called the patterns that account for the most variance in the data *Empirical Orthogonal Functions* (EOFs).

The EOF technique has the following advantages:

- The main patterns of variability are defined by the data themselves, thereby giving reason to believe that they are "physically significant."
- Because the patterns are linearly independent (orthogonal), the original patterns of variability (and their spatial derivatives) can all be approximated by linear combinations of features.

It also turns out that EOFs may reveal artifacts in the data introduced by the instrument used to collect the data.

In addition to the Jones et al. (1991) analysis technique that was reported during the course of the project, new types of data also influenced the research direction. Two data sets were particularly important. First, was a set of detailed, three-dimensional wind observations provided by Schneider (1991), and second were detailed estimates of transmittance through a smoke plume presented as two-dimensional imagery (Bleiweiss et al., 1991). Transmittance inhomogeneities through a plume represent an important class of problem for the Army. Unfortunately, the data were obtained only a few months before the conclusion of the project, preventing as comprehensive an analysis as desired.

Considerable effort was spent in developing vector-analysis techniques for application to the detailed wind observations in the belief that an understanding of the atmospheric motions would provide a basis for describing the inhomogeneities of the scalar distributions. While this

still is a reasonable expectation, it became apparent while developing the vector-analysis techniques that this approach would require more effort than could be expended as part of the current project; therefore, the focus returned to the analysis of scalar distributions. Although the main focus of this report is on the distribution of scalars in the atmosphere, some of the vector-analysis approaches and preliminary results are also discussed.

Some conclusions can be drawn from the studies reported here, but to a large extent they are only preliminary. Some of the techniques appear promising, but have not been refined and applied rigorously enough at this stage to realize that promise. Thus, some of the conclusions reported at the end of this report take the form of suggestions for refinements and future applications of the techniques described here.

II REVIEW OF FRACTAL CONCEPTS AND THEIR APPLICATIONS TO THE ATMOSPHERE

This section is in large part derived from a review published earlier (Ludwig, 1989), but inasmuch as this is a rapidly evolving topic it has been necessary to include some more recent material. The purpose of the review is to provide definitions for fractal dimension and descriptions of various methods by which it can be calculated. Another important goal is to provide a basis for understanding why the concept of fractals has relevance to the understanding of atmospheric inhomogeneities.

The word "fractal" only appeared about 16 years ago (Mandelbrot, 1975). The widespread use of the word in popular and technical writing in recent years suggests that either fractal concepts have general applicability, or that fractals have taken on something of a cult status. The fact is that both reasons apply: Concepts related to fractals do provide good mathematical analogs in fields ranging from cosmology to geography to population biology and fluid mechanics (Mandelbrot, 1983); unfortunately, there may also have a been a tendency to think that this widespread applicability meant that a "universal truth" had been found. Atmospheric science is among those places where the fractal has found a home. The ability of fractal concepts to describe a wide variety of conditions and processes is tantalizing, but to date, the practical, predictive results have been few.

This review is intended to provide a qualitative understanding of important concepts and an introduction to the simplified version of the mathematics underlying these concepts. Examples of how the concepts apply to the atmosphere, and how some relate to classical approaches are also included.

A. GENERAL CONCEPTS

One of the more comprehensible parts of many discussions of turbulence is the following piece of doggerel credited to Richardson (1922):

> *Big whorls have little whorls,*
> *Which feed on their velocity;*
> *And little whorls have lesser whorls,*
> *And so on to viscosity...*

Those four lines provide a vivid picture of turbulence; they also provide a good starting point for visualizing fractals. If we examine the streamlines associated with Richardson's big and little whorls, we find that those streamlines have their corresponding large, little, lesser, and least wiggles—down to where "viscosity" stops the process. We can magnify and find wiggles superimposed on wiggles already there. This is one type of fractal. In this case, we have a collection

of points that form a line with wiggles and roughness over a large range of scales. The set of points could also be part of a surface with roughness elements at every scale, or a collection of separated points that are arranged in clusters of clusters of clusters...

Many lines and surfaces in nature are fractals. Coastlines have the property of being "rough" over a wide range of scales (Mandelbrot, 1983; Feder, 1988). Lovejoy (1982) found that cloud and rain areas have these properties over more than four orders of magnitude; Rys and Waldvogel (1986) looked at hailstorm perimeters and obtained similar results down to sizes of a few kilometers, but found smoother outlines at smaller scales.

Fractals are rough geometric shapes: their roughness is qualitatively similar at all scales; the measure of roughness is fractal dimension. Later I discuss several quantitative mathematical expressions that can be used to determine fractal dimension; here I limit the discussion to some easily understood subjective attributes associated with fractal dimension, such as the already noted relation between fractal dimension and perceptions of roughness. Pentland (1984) reported that when people ranked images of surfaces in order of their perceived roughness, the rankings corresponded to fractal dimension, with the roughest surfaces having the highest fractal dimension.

Space-fillingness is another useful subjective concept associated with fractal dimension. A smooth line is confined to one dimension, a smooth surface to two. A fractal, with its wiggles on wiggles on wiggles, begins to infringe on other dimensions. Topologically, the fractal line or fractal surface may have only one or two dimensions, but the wiggles make them substantively different from the smooth shapes. Fractal dimension provides a quantitative measure of the degree to which these structures fill the physical space beyond their topological dimension.

The concepts discussed above can be extended to any number of dimensions, but considerable care must be taken when the dimensions represent different physical properties (e.g., a mix of pressure, density, and wind components). Even in two dimensions (e.g., a time series of aerosol concentrations at a point), Mandelbrot (1985) warns that there can be discontinuities in certain measures related to fractal dimension.

B. MATHEMATICAL RELATIONSHIPS

Several different definitions of fractal dimension are found in the literature. They illustrate different physical properties or processes that are related to fractal dimension. The first two methods for defining and calculating fractal dimension discussed below follow from the fact that fractal dimension is a measure of space-filling properties. The other definitions are related to the fact that fractals are associated with fields that are self-similar (i.e., scaling) over a wide range of scales.

1. Box (or Cell) Counting

Mandelbrot (1975) defined fractal dimension through its relation to the space-filling concept. He assumed a continuous distribution of some parameter so that there are isosurfaces

containing all the points with the same parameter value. He then invoked a concept commonly used for measuring metric properties by counting the number of elementary units (e.g., small units of area or volume) required to cover all the points in the set. Restated, a metric property, M, is estimated by counting the number (N) of measurement units of linear size λ that are required to cover the set of points being measured. For simple shapes, the measure is related to the dimension, D, of the shape and the size of the measurement unit:

$$M = N\lambda^D \quad . \tag{1}$$

Mandelbrot (1983) has noted that the usual smooth shapes of Euclidian geometry result in integer values for D, but many natural shapes require D to be fractional to obtain consistent results. The fractional (fractal) dimension D in these cases is analogous to the Euclidian dimension in terms of its relation to the metric properties of a surface.

In his extension of the measuring concept outlined above, Mandelbrot starts with a large cube containing part, or all, of a surface whose fractal dimension is to be determined. He defines the side of that cube as the external scale, L, and then subdivides it into smaller cells of side length ℓ counting the number of smaller cells containing at least one point on the surface. If the "surface" is a straight line, the number of small cells through which it passes is proportional to $(L/\ell)^1$. A flat plane will intercept a number of small cells that is approximately proportional to $(L/\ell)^2$. For a solid "surface," that number of cells is proportional to $(L/\ell)^3$. In each example, the exponent of (L/ℓ) is the Euclidian dimension of the surface, confirming the analogy to the usual measurement concepts. However, the exponent assumes fractional values for rough, scaling objects. For example, a line that has many wiggles, with wiggles upon those wiggles, passes through a number (N) of small cells that is approximated by

$$N = k\,(L/\ell)^D \quad , \tag{2}$$

where k is a proportionality constant and D, the fractal dimension, is larger than 1. Similarly, for a rough plane with an irregular surface over a wide range of scales, D is larger than 2.

Greenside et al. (1982) attributed an algorithm for computing fractal dimension based on Mandelbrot's (1975) definition outlined above to Takens (1981). They found the approach to be impractical for surfaces of dimension larger than two because of convergence problems. Later in this report, applications of this approach to two-dimensional scalar fields are presented. In these applications, the scalar values were rescaled to fall within the same numerical range as the linear dimensions of the area over which they were measured. This allowed the use of cubes to cover the scalar surface.

When the definition provided by Eq. (2) is reduced to two dimensions, a square and smaller squares replace the cube and subcubes; the definition then can be used to examine the lines formed when a plane intersects a fractal surface. It is generally accepted (Mandelbrot, 1983) that if a fractal shape is intersected by a flat surface of lower dimension, the intersection is also a fractal. The dimension of that fractal differs from that of the original object by the integer difference between the dimensions of the two spaces. This fact could be used to examine the distributions of scalars in space by applying it to an isoline (line of constant scalar value), which is the intersection of a surface whose height is proportional to the value of some parameter at that x, y

location in the underlying plane. Thus, the cell-counting method could be used to infer fractal dimension of a parameter distribution from the fractal dimension of an isoline. There are pitfalls in this method when the intersecting plane is not one of constant parameter value, or the units of x and y are different.

The cell-counting concept is reasonably direct and easily applied to an array of discrete numbers (e.g., a digitized image). The constants for the logarithmic form of Eq. (2) are found by linear regression:

$$\log (N) = \log (k) + D \log(L/\ell) \tag{3}$$

In practice, we want as many values for N as possible. For a discrete array, each value must correspond to an integer value of (L/ℓ). Therefore, the calculations that are described later used a large area that was defined so that L had many divisors. The large number of divisors was obtained hy defining L as a product of powers of 2, 3, and 5.

2. Area/Perimeter Methods

Another method for calculating fractal dimension that is related to the space-fillingness of a curve uses the relationship between the area A enclosed by some shape and its perimeter P. A smooth perimeter encloses a larger area than the same wiggly length. For smooth curves, the perimeter P is proportional to the square root of the enclosed area, but a fractal shape encloses an area related to its perimeter by

$$P \sim \sqrt{A^D} \quad , \tag{4}$$

where D is the fractal dimension. Eqn. (4) applies to isopleths and their enclosed areas, so it can also be used for estimating the fractal dimension of a scalar field. The data available for this study did not lend itself easily to the identification of isopleths on a fine scale; thus, this technique was not implemented.

3. Scaling and Probability Distributions

Although fractals are geometric shapes, their potential applications as descriptors of natural phenomena frequently arise in connection with highly irregular spatial or temporal distributions of some nongeometric quantity such as kinetic energy, aerosol concentration, or temperature. Jones et al. (1991) distinguish between two distinct types of fractal dimension:

- The fractal dimension of the graph of some fluctuating function
- The fractal dimension of the set of points that define active regions of fluctuation.

The second, geometric definition is addressed by the two methods described in the preceding sections. While it is possible to convert a problem involving the first type of fractal dimension into one involving the second type by examining shapes of isopleths as described above, it is often more useful to invoke statistical descriptions. For example, one common statistical descriptor is the probability distribution $Pr[\Delta c(\Delta r) > q]$ associated with differences in parameter value over a specified distance. Pr [r > s] is the probability that the argument inequality is true;

$\Delta c(x)$ is the absolute value of the difference in c at two points separated by a distance x. These probability distributions vary according to the separation distance. Generally, the likelihood of exceeding some specified difference increases with increasing separation between points. For many natural phenomena, the probability distributions retain the same functional form for different separations, but exhibit a change of scale. This is because many natural fields vary in such a way that the fluctuations look qualitatively the same, regardless of magnification. Large-scale fluctuations in a scaling field are qualitatively the same as the middle-scale fluctuations embedded within them, which are in turn similar to the still smaller fluctuations.

When a field is scaling, the probability distributions for different separations are related as follows:

$$\Pr [\Delta c(\lambda \Delta r) > q] = \Pr [\lambda^{H} \Delta c(\Delta r) > q] \quad . \tag{5}$$

Equation 5 shows that the fluctuations in c over small separation distances Δr are related to those at larger separations ($\lambda \Delta r$) by the factor λ^{H}. The exponent H is the Hausdorff dimension, which is related to the fractal dimension D and the number of Euclidian dimensions E of the space where the field is plotted (Voss, 1988) by:

$$D = 1 + E - H \quad . \tag{6}$$

For example, a time series (where time is the dimension against which the variable is plotted and E = 1) has a fractal dimension of 2–H. When the probability of the difference exceeding some selected value is directly proportional to the separation, as it is for a steadily increasing or decreasing variable, then H is 1 and the fractal dimension is also 1—that is, a smooth line for the time series. If H approaches 0, the fractal dimension approaches 2 and the difference in value at two points is almost as likely to exceed a specified amount for closely spaced points as it is for widely spaced points. This is characteristic of a very rough, space-filling time-series graph.

Schertzer and Lovejoy (1983) assumed a functional form for the upper tails of atmospheric probability distributions in order to use Eqs. (5) and (6) to estimate fractal dimension from observed data. Often, the tail of a distribution is most interesting because it involves the large, infrequent fluctuations. They assumed that the upper tail had a hyperbolic form; that is, for large q:

$$\Pr [\Delta c > q] = F(q) \tag{7}$$

where Schertzer and Lovejoy (1983) define F(q) by:

$$F(q) = K q^{-\alpha} \quad . \tag{8}$$

The constants H and α are estimated from the data after substituting Eq.(8) in Eq. (5) and taking logarithms:

$$\log \{ \Pr [\Delta c (\lambda \Delta r) > q] \} = k + H \log(\lambda) - \alpha \log(q) \quad . \tag{9}$$

This equation is applied to observed data as follows:

(1) α and $[k + H \log(\lambda)]$ are determined by linear regression from the upper tail of the distribution for each λ.

(2) The average α is determined; if individual values of α do not differ widely, the average α is used to get an equation relating λ and H for each value of q so that linear regression can be used to determine H.

(3) D is then obtained from Eq. (6).

The hyperbolic functional form for the upper tail was chosen by Schertzer and Lovejoy (1983) because it appears to fit atmospheric distributions that they analyzed. Other functional forms can be used in much the same way as described above. The important point is that the probability distributions are the same if the separation distances and parameter values are scaled as in Eq. (5).

4. Spectral Analysis

The method just described, which relates the difference in the value of a parameter at two points to the separation between those points, is closely related to the estimation of spatial autocorrelation. Not surprisingly, therefore, spectral-analysis methods can be used to estimate the Hausdorff and fractal dimensions for fractal Brownian functions defined by Eq. (5). For example, the exponent of the power spectrum ($-\gamma$) for a scaling time-series graph is related to the Hausdorff dimension (Saupe, 1988) by

$$\gamma = 2\,H + E \tag{10}$$

When we combine Eqs. (5) and (10) and suhstitute E = 1 (for a time-series graph), we get $\gamma = 5 - 2\,D$. The spectral density P(f) of a scaling variable is proportional to f^{2D-5}, where f is frequency.

The spectral relationship can also be used for estimating the fractal dimension of a scaling, isotropic field in two or three dimensions. Fast-Fourier-transform (FFT) methods give the amplitudes of the Fourier terms in wave-number space. The spectrum is then fit without regard to direction. In essence, the procedure averages the amplitudes around circles (or spheres) of constant wave-number radius. Pentland (1984) used the spectral method to characterize the fractal dimensions of 16×16 pixel subsections of photographs, and used the results as a basis for distinguishing between different picture areas according to their texture. For these two-dimensional images, the power density scaling is proportional to f^{2D-8}.

The spectral approach proved the least successful of those that were implemented for these studies. However, an inverse Fourier transform approach described later proved quite useful for generating test arrays of known fractal dimension.

5. Multiresolution Feature Analysis

If fractals represent a composite of similar "features" over a broad range of scales, then it should be possible to use this fact to estimate fractal dimension. This is the essence of the approach described by Jones et al. (1991). The following description of the methodology, taken from Jones et al. (1991), is a variation of the method based on probability distributions that was discussed earlier. Instead of simply using changes in the value of the dependent variable as a

function of distance, they express those changes in the form of a set of differences that can be used to define geometric "features" of the distribution. They also degrade the image resolution to get different separation distances. This approach provides a method by which fractal dimension can be more easily related to specific physical characteristics of the field.

The process begins by producing an image of half the original resolution through low-pass filtering. Correlation with a centered 3×3 matrix gives a value for each point. These new values are resampled at every other grid point in both directions, giving one point for each four in the original array and a new image of half the resolution (and about half the grid points in each direction). The process is repeated to obtain a set of images covering a range of resolutions.

Jones et al. (1991) found empirically that preprocessing of the original image to introduce slight smoothing helped them obtain better scaling in their analyses of LANDSAT imagery. Following their example, the data were initially smoothed with the following matrix:

$$\mathcal{L}_0 = \begin{bmatrix} 0.031 & 0.044 & 0.031 \\ 0.044 & 0.7 & 0.044 \\ 0.031 & 0.044 & 0.031 \end{bmatrix} . \tag{11}$$

The smoothings to obtain the reduced-resolution imagery used the matrix

$$\mathcal{L}_1 = \begin{bmatrix} 0.0625 & 0.125 & 0.0625 \\ 0.125 & 0.25 & 0.125 \\ 0.0625 & 0.125 & 0.0625 \end{bmatrix} , \tag{12}$$

After the set of reduced resolution images have been obtained, a high-pass filter is applied to each image. The high-pass filter can be interpreted as a "feature detector": It returns large positive or negative numbers when superimposed on a pattern in the image that corresponds to the feature it is designed to detect. For example, the following matrices detect "edges" oriented vertically and peaks (or holes) in the pattern:

$$\mathcal{H}_{\text{vert edge}} = \begin{bmatrix} 1 & 0 & -1 \\ 1 & 0 & -1 \\ 1 & 0 & -1 \end{bmatrix} \tag{13}$$

and

$$\mathcal{H}_{\text{peak}} = \begin{bmatrix} -1 & -1 & -1 \\ -1 & 8 & -1 \\ -1 & -1 & -1 \end{bmatrix} . \tag{14}$$

The matrices can be combined. For instance, the outputs from four edge detectors (for vertical, horizontal, and two orientations of diagonal edges) can be summed to find regions of strong gradients.

After arrays of feature intensities have been obtained for the different resolution images, the maxima and minima are identified. Then the numbers of these extremes whose absolute values

exceed various thresholds are counted. Plots of these thresholds and numbers of extrema exceeding them for each resolution can serve as a basis for estimating fractal dimension. The fractal dimension of the graph of a fluctuating function C is the measure that is most closely related to the scaling properties of C. According to Eq. (5) self-similar scaling processes display amplitude fluctuations (ΔC) whose magnitudes tend to be proportional to the ratio of their spatial scales λ raised to a power, H. Jones et al. (1991) refer to H as the *similarity parameter*. In essence, the process described above identifies the number (or probability) of fluctuations of certain type exceeding various thresholds at different resolutions.

The process described above provides an estimate of $(n_q)_i$; the number of exceedances (for a given total area) of threshold q for the i^{th} resolution $\lambda_i \Delta r_0$, where Δr_0 is the cell size in the original data set. If the distribution is self similar, then the number of features exceeding a given threshold q will satisfy a relationship of the following form:

$$\lambda_i^2 (n_q)_i = q\lambda_i^{-H} \quad , \tag{15}$$

Jones et al. (1991) choose a series of values for H and estimate fractal dimension based on which of those values produces the best coincidence of the graphs for the different resolutions. Examples of the method are given later.

6. Anisotropic Effects

The above discussions all assume that the relationships are both independent of direction and scale. This is not necessarily the case. Differences between scaling of feature dimensions in the vertical and horizontal directions seem likely to occur in a medium that is as highly stratified as the atmosphere. It turns out that many of the fractal properties of the atmosphere arise from the cascade of energy down through the various scales of motion. A fractal dimension that applies over the complete range of scales implies that the ratios of the number of eddies to subeddies remains constant over that range, which need not be true. While this report has not attempted to incorporate these effects into the analyses presented later, completeness requires that they be discussed.

a. Self-Affine Distributions

The analytical techniques discussed above are appropriate for shapes with self-similar characteristics, that is, for those cases where the irregularities at all scales are similar in the Euclidian geometry sense. The smaller-scale features are contracted (and perhaps rotated) versions of the larger irregularities, but they maintain their proportions and the corresponding angles do not change. These cases are a subset of a more general class of shapes that occur naturally, the self-affine fractals, where the smaller-scale irregularities are affine transformations of those at larger scales. Barnsley and Sloan (1988) described affine transformations as "combinations of rotations, scalings, and translations of the coordinate axes in n-dimensional space." Voss (1988) defines self-affinity as nonuniform scaling, i.e., different scaling along different axes (directions). Mandelbrot (1985) pointed out that the methods described above for calculating fractal dimension are not always appropriate for this more general class. In particular, he notes that the time

history of a scalar involves a choice of units for both time and the scalar; different results may be obtained for different choices of units. There will be local and global fractal dimensions. In fact, Mandelbrot (1985) defines three versions of fractal dimension corresponding to different methods for estimating them. The three different dimensions are the same for self-similar sets, but differ for self-affine sets. Mandelbrot (1985) explained that (for the time series of some parameter, B)

> *..."square," "distance," and "circle" are vital notions in isotropic geometry, but they are meaningless in affine geometry. More precisely, they are meaningful for relief cross-sections, but are meaningless for [B] noises, because the units along the t-axis and the B-axis are set up independently of each other, hence Δt and ΔB cannot be combined. There is no intrinsic meaning to the notion of equal height and width, a square cannot be defined. Similarly, a circle cannot be defined because its square radius $R^2 = \Delta t^2 + \Delta B^2$ would have to combine the units along both axes. Furthermore, one cannot 'walk a compass' along a self-affine curve because the distance covered by each step combines a Δt and a ΔB.*

The above discussion emphasizes the care that must be taken when applying what are essentially geometric measurement techniques to the problem of estimating a fractal dimension. Although two of the techniques described by Mandelbrot (1985) give results in the small scale that are consistent with the results obtained for self-similar sets, it is wise to apply the techniques carefully to avoid the inconsistencies enumerated above. Even then, anisotropy in the processes producing the sets can make new measures necessary. One of these is discussed in the next subsection.

b. Elliptical Dimension

The horizontal scales of atmospheric motion are much less constricted than the vertical. This causes anisotropy in atmospheric turbulence, especially at the larger scales. It also suggests that the transfer of energy from large eddies to smaller eddies is not likely to be self-similar, but rather self-affine, even though the vertical and horizontal distance units are the same. Schertzer and Lovejoy (1983, 1987; also Lovejoy and Schertzer, 1986) noted the following important facts regarding mesoscale atmospheric processes:

- The energy spectrum is scaling (i.e., it has the form k^{β_h}, where k is the wave number and $\beta_h = 5/3$ is the appropriate value for wave numbers in the horizontal plane).
- The energy spectrum for wave numbers in the vertical plane is also scaling, but anisotropy makes the relevant exponent, β_v, quite different: $\beta_v = 11/5$.
- There is extreme variability, because active regions that account for most of the energy and moisture flux are sparsely distributed.

To deal with the above observations, Lovejoy and Schertzer (1986) modified the self-similar concepts to apply them to the anisotropic case. In extending the concepts, they assumed that there is a constant energy flux over the range of scales of interest, and that there are rules for describing how the statistical properties of eddies are transformed from one scale to another. In

dealing with anisotropic eddies, both shape and dimension must be characterized. Schertzer and Lovejoy (1987) represented the anisotropic scaling in a manner similar to that discussed earlier for the isotropic case, except that horizontal and vertical scaling were considered separately, that is,

$$\Pr [\, \Delta c(\lambda \Delta x) > q \,] = \Pr [\, \lambda^{H_h} \Delta c(\Delta x) > q \,] \tag{16a}$$

$$\Pr [\, \Delta c(\lambda \Delta y) > q \,] = \Pr [\, \lambda^{H_h} \Delta c(\Delta y) > q \,] \tag{16b}$$

$$\Pr [\, \Delta c(\lambda \Delta z) > q \,] = \Pr [\, \lambda^{H_v} \Delta c(\Delta z) > q \,] \tag{16c}$$

or

$$\Pr [\, \Delta c(\boldsymbol{\mathcal{T}} (\Delta \mathbf{r}) > q \,] = \Pr [\, \lambda^{H_h} \Delta c(\Delta \mathbf{r}) > q \,] \tag{17}$$

where

$$\boldsymbol{\mathcal{T}} = \begin{bmatrix} \lambda & 0 & 0 \\ 0 & \lambda & 0 \\ 0 & 0 & \lambda^{H_z} \end{bmatrix} \tag{18}$$

$$H_Z = (H_h / H_v) \tag{19}$$

and

$$\Delta \mathbf{r} = \begin{bmatrix} \Delta x \\ \Delta y \\ \Delta z \end{bmatrix} . \tag{20}$$

The matrix $\boldsymbol{\mathcal{T}}$ produces a magnification overall, with stretching in the z direction; it transforms the probability distributions and introduces an elliptical geometry to account for the different horizontal and vertical scalings. Figure 1 shows how the magnification and stretching relates the small, vertically oriented shapes (eddies in this case) to a large, horizontally oriented shape. The transformation changes the volume by a factor $\lambda^2 \lambda^{H_z} = \lambda^{D_{el}}$, where $D_{el} = 2 + H_z$. Lovejoy and Schertzer (1986) called D_{el} the elliptical dimension. In an isotropic system, $H_Z = 1$, and therefore the elliptical dimension equals 3. For two-dimensionally isotropic sets $H_z = 0$ and $D_{el} = 2$. Schertzer and Lovejoy (1987) described a technique called *functional box counting* for determining elliptical fractal dimension from observed data.

C. HOW FRACTALS MAY DEVELOP

To this point, the discussion has focused on definitions of fractals and related concepts, while giving little attention to their underlying physical causes. At least three types of evidence indicate a connection between fractals and atmospheric processes:

- The structure of turbulent eddies observed in flow visualization experiments

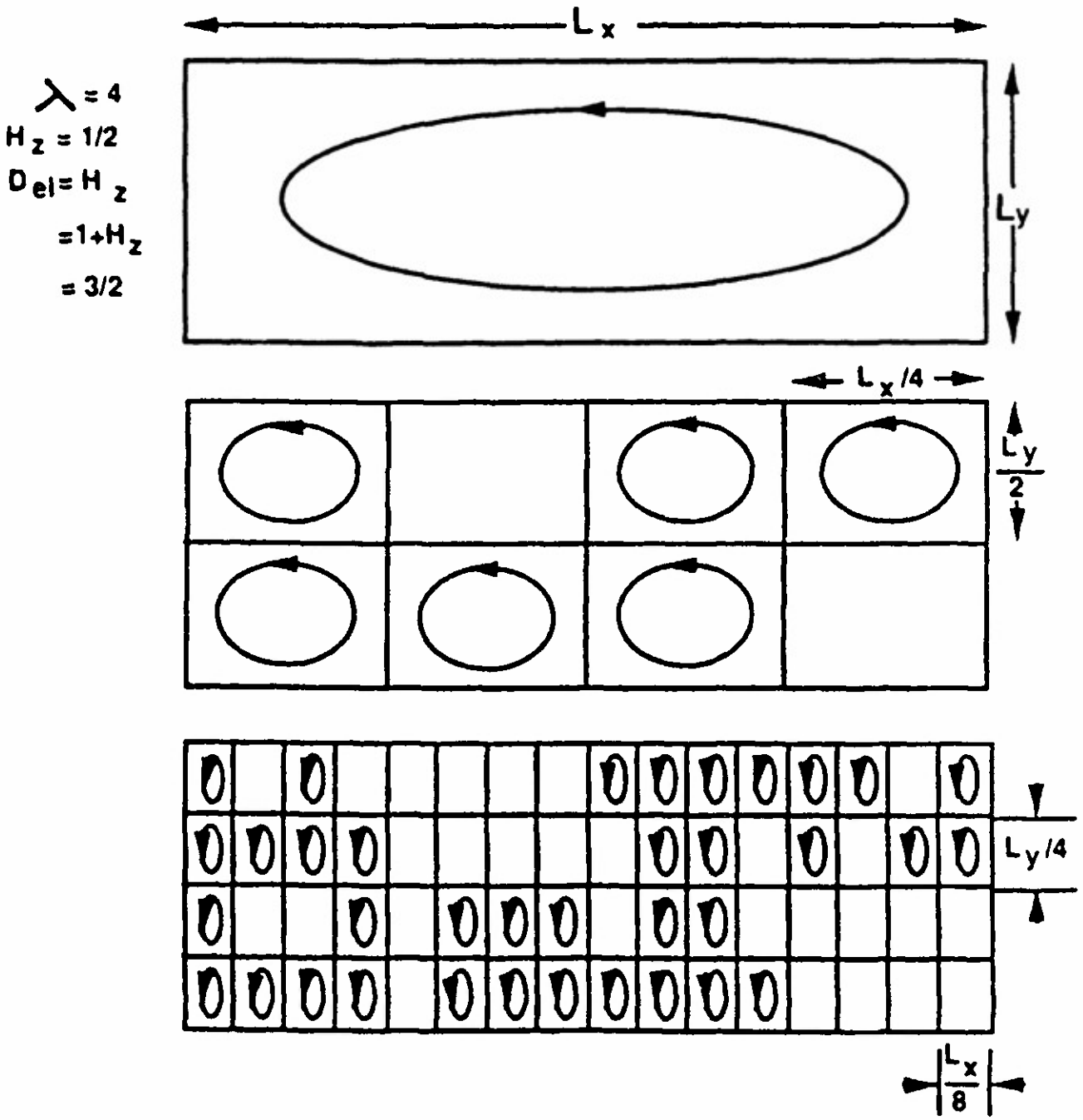

FIGURE 1 SCHEMATIC DIAGRAM ILLUSTRATING THE CONCEPT OF ELLIPTICAL FRACTALS
After Lovejoy and Schertzer, 1986

- Similarity arguments from classical turbulence theory
- Detailed numerical flow simulations.

These are discussed in the following sections.

1. Observational Evidence

a. Shear-Layer Flow

Van Dyke (1982) showed several examples of structure in the turbulent layer that forms in the shear zone between fluids flowing at different velocities. The structure that commonly occurs in such flows is evident. Reynolds (1985) provided the basis for a qualitative discussion of the processes involved. Although his notes do not mention fractals, they do give evidence of scaling and the development of self-affine structures of different scales in the motion field.

Figure 2 is based on Reynolds' (1985) schematic diagram showing free shear flow. Initially, vorticity is produced at the tip of the separator that is used to generate the flow. An unstable two-dimensional shear layer is formed. Instabilities excited by slight vibrations grow rapidly so that vorticity is quickly concentrated in nearly discrete vortices, oriented generally perpendicular to the flow direction. Not all vorticity is in the major features; some remains in "braids" connecting the major vortices (Figure 2), where it is stretched as the large-scale vortices "wind in" the fluid between them. This intensifies the vorticity in the braids, forming new vortices with axes aligned along the principal strain direction, as shown in Figure 3. These vortices undergo the same processes described above, but on a smaller scale and with different orientation. One can expect that the new, smaller vortices also contain irregularities where new minibraids form and stretch vortices along new strain axes. These new structures can undergo similar deformation on a still smaller scale, so that the processes continue to produce self-affine structures from the outer scale defined by the largest vortices down to the scale of viscous dissipation.

The consequence of this process appears to be a set of vortices on vortices on vortices and so on, much like Richardson's (1922) description. Analogous reasoning can be applied to other flow types such as jets, boundary layers, and wakes, which are also characterized by regions of strong shear and concentrated vorticity.

b. Turbulent Diffusion

Procaccia (1984) reviewed the effects of fractal turbulence structures on turbulent diffusion, fluctuations of passive scalars, electromagnetic wave propagation, and cloud perimeters. He examined the behavior of the interparticle separation distance, $\mathbf{R} = \mathbf{r}_1 - \mathbf{r}_2$, of two points caused by their relative velocity, $\mathbf{V}(t) = \mathbf{V}_1 - \mathbf{V}_2$:

$$\mathbf{R}(t) = \mathbf{R}(0) + \int_0^t \mathbf{V}(\tau)\, d\tau \quad . \tag{21}$$

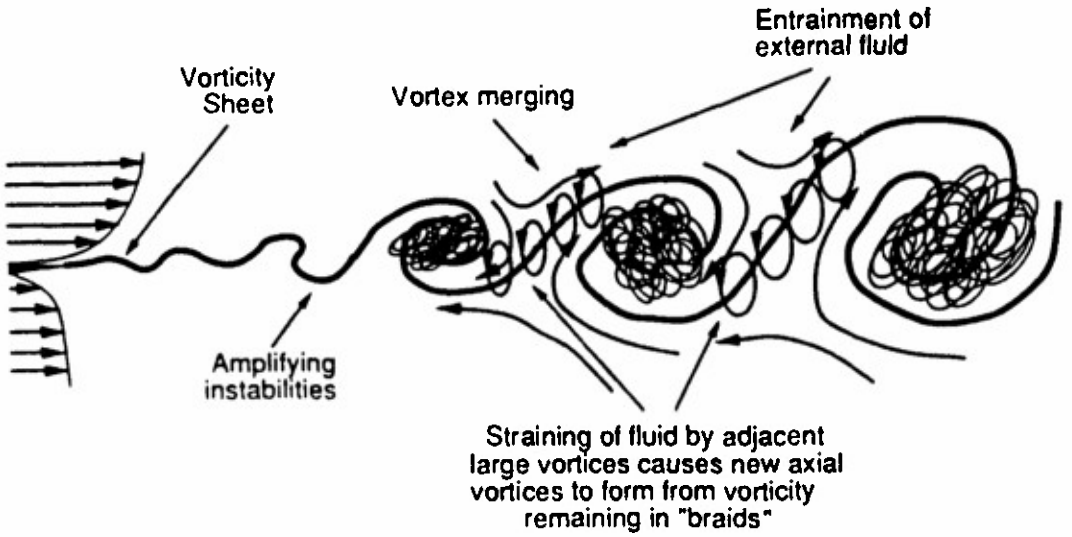

FIGURE 2 VORTEX BRAIDS BETWEEN SHEAR FLOW EDDIES

After Reynolds, 1985

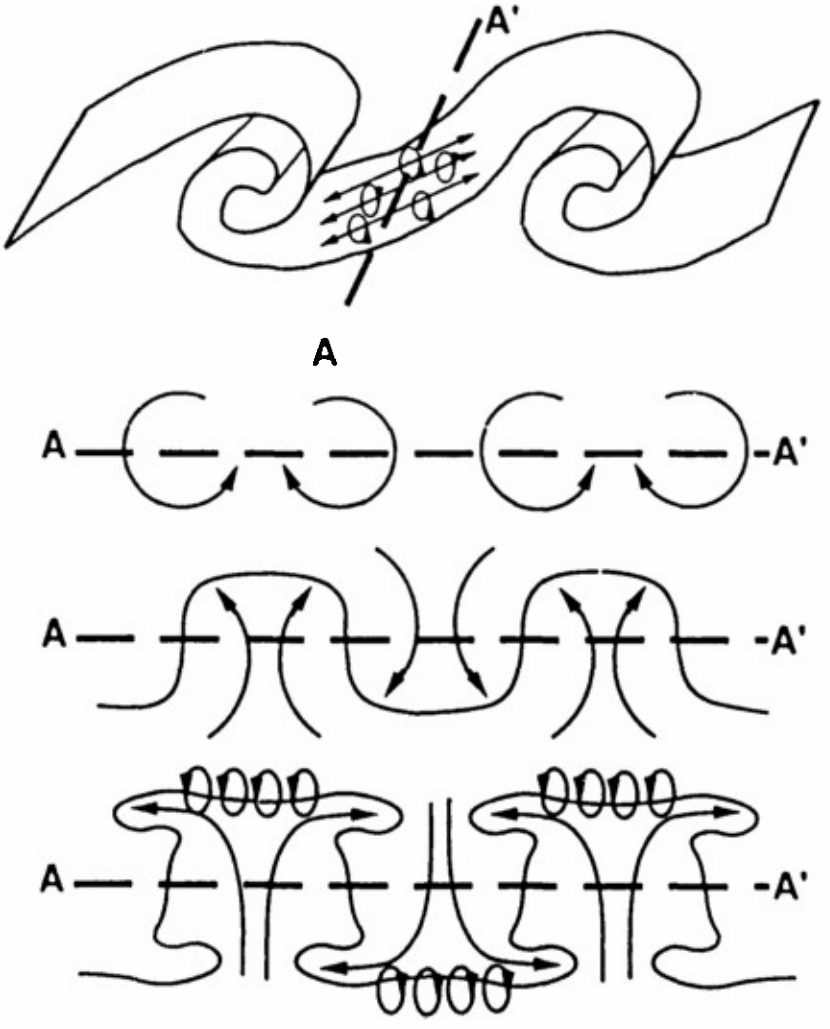

FIGURE 3 ENERGY TRANSFER TO SMALLER EDDIES BY VORTEX STRETCHING

After Reynolds, 1985

For isotropic turbulence, the ensemble average separation—represented by angle brackets, < > is constant and equal to the initial separation because $< \mathbf{V}(t) > = 0$, but variance, $< \mathbf{R}^2 >$, changes:

$$\frac{d}{dt}\left\langle R^2 \right\rangle = 2\int_0^t \left\langle \mathbf{V}(t) \cdot \mathbf{V}(\tau) \right\rangle d\tau \quad . \tag{22}$$

Procaccia (1984) asserted that, although the correlation $< \mathbf{V}(t) \cdot \mathbf{V}(\tau) >$ is nonstationary, some function, g(x), of scaled time variables exists such that

$$\left\langle \mathbf{V}(t) \cdot \mathbf{V}(\tau) \right\rangle = \left\langle \mathbf{V}(t) \cdot \mathbf{V}(t) \right\rangle g\left(\frac{t-\tau}{t_R}\right) \quad , \tag{23}$$

where t_R is the typical decay time for velocity differences over a length scale, R. Substituting in Eq. (22) provides asymptotic predictions at extreme times:

$$\frac{d}{dt}\left\langle R^2 \right\rangle = \begin{cases} \left\langle \mathbf{V}(t) \cdot \mathbf{V}(t) \right\rangle t & t << t_R \\ \left\langle \mathbf{V}(t) \cdot \mathbf{V}(t) \right\rangle t_R & t >> t_R \end{cases} \tag{24}$$

The diffusivity, $d < R^2 > /dt$, can be determined from $< \mathbf{V}(t) \cdot \mathbf{V}(t) >$ when R is in the inertial range. The ratio of the separation distance, R, to a typical velocity difference over that distance defines t_R. For the "homogeneous fractal model" of turbulence described below,

$$\langle \mathbf{V} \cdot \mathbf{V} \rangle \sim (\bar{\varepsilon} R)^{\frac{2}{3}} \left(\frac{R}{\ell_0}\right)^{\frac{3-D}{3}} \quad , \tag{25}$$

where ℓ_0 is the outer scale of the turbulence. Procaccia (1984) used this assumption to obtain

$$\frac{d}{dt}\left\langle R^2 \right\rangle \sim \begin{cases} \bar{\varepsilon}^{1/3} R^{4/3} (R/\ell_0)^{(\frac{1}{2} - \frac{D}{6})} & t << t_R \\ \bar{\varepsilon}^{1/3} R^{4/3} (R/\ell_0)^{(2 - \frac{2D}{3})} & t >> t_R \end{cases} \tag{26}$$

where R is the root-mean-square separation. For space-filling turbulence, where D = 3, the above expressions reduce to the classical "4/3 law."

Hentschel and Procaccia (1983) examined Gifford's (1957) and Richardson's (1926) two-point diffusion data and obtained estimates for D between 2.5 and 2.78, from which they concluded that these were reasonable values that supported the "fractally homogeneous turbulence" concept.

c. Cloud and Rain Perimeters

As noted earlier, Lovejoy (1982) found that cloud and rain area perimeters were fractals over a range of six orders of magnitude—from about 1 km^2 to 10^6 km^2. The fractal dimension of the perimeter was $\overline{D} = 1.35 \pm 0.05$, so the fractal dimension of the cloud surface was 2.35 ± 0.05 in the isotropic case. Procaccia (1984) considered how a surface defining the outer boundary of the cloud would be distorted by turbulent diffusion, and concluded that the fractal dimension, D_c, of the cloud perimeter is given by

$$D_C = (11 - D)/6 \quad , \tag{27}$$

where D is the fractal dimension of the turbulence. Using a value of 2.6 for the fractal dimension of the turbulence (Hentschel and Procaccia, 1983) gives $\overline{D} = 1.4$, in agreement with Lovejoy's (1982) value.

d. The Boundary of a Diffusing Scalar In a Turbulent Flow

Prasad and Sreenivasan (1990) experimentally examined several aspects of turbulence for fractal characteristics. They measured the concentration field of a diffusing fluorescent material in water. Their technique used a sheet of laser light to induce fluorescence. The fluid was scanned very rapidly and two-dimensional images obtained from closely spaced planes. Subsequent computer processing provided the three-dimensional distribution of the material. Among the characteristics that Prasad and Sreenivasan (1990) examined was the shape of the interface between the fluorescent material and the surrounding water. They found that the interface was very rough, and generally self-similar with a fractal dimension of 2.35 ± 0.04.

e. Elliptical Fractals

Schertzer and Lovejoy (1983) introduced the concept of elliptical fractal dimension because it provides a smooth transition from the very large, horizontally oriented, "Hadley-like" cells down to the vertically oriented convective cells. An analysis (Lovejoy et al., 1987) of radar precipitation data showed that rainfall is distributed in space with an elliptical fractal dimension of about 2.22. The elliptical fractal dimension represents the ratio of horizontal contraction to vertical, so this suggests that rainfall is more horizontally stratified than are the air motions, which the authors estimated as having a fractal dimension of about 2.56 (Lovejoy et al., 1987).

2. Classical Turbulence Theory

The description by Frisch et al. (1978) of the "β-theory" of turbulence provides a good physical picture of the turbulent cascade. The energy spectrum E(k) is defined as the kinetic energy per unit mass per unit wave number k. For purposes of argument, consider a spectrum of eddies beginning at the largest scale, ℓ_o, where the energy is introduced, and proceeding to successively smaller, discrete sizes, ℓ_n, as follows:

$$k_n = 1/\ell_n = 2^n/\ell_o \qquad n = 0, 1, 2, 3, \ldots \tag{28}$$

If E_n is the discretized kinetic energy per unit mass in the wave numbers near k_n, it can be defined in terms of a characteristic velocity v_n. This characteristic velocity is not total velocity, but the velocity difference for the eddy size ℓ_n:

$$E_n \sim v_n^2 \quad . \tag{29}$$

The eddy turnover time t_n is given by

$$t_n \sim \ell_n / v_n \quad , \tag{30}$$

Frisch et al. (1978) defined an energy (per unit mass) transfer rate, ε_n, from eddies of wave number k_n to k_{n+1} for the inertial subrange, where t_n is much greater than the viscous dissipation time, ℓ_n^2/ν (ν is kinematic viscosity), and much less than the characteristic time for the larger scale motions, ℓ_o/v_o:

$$\varepsilon_n \sim E_n/t_n \sim (v_n)^3/\ell_n \quad . \tag{31}$$

For statistically stationary turbulence, energy introduced at large scales (ℓ_o) transfers to successively smaller scales until the dissipation scale, ℓ_d, is reached and the energy dissipation rate, ε_n, is a constant, $\bar{\varepsilon}$. Solving for v_n and E_n gives

$$v_n \sim (\bar{\varepsilon}\ell_n)^{\frac{1}{3}} \tag{32}$$

$$E_n \sim (\bar{\varepsilon}\ell_n)^{\frac{2}{3}} \quad . \tag{33}$$

Equations (33) and (34) are the same as Kolmogorov's results. A Fourier transformation provides the wave-number spectrum:

$$E(k) \sim (\bar{\varepsilon})^{\frac{2}{3}} k^{-\frac{5}{3}} \quad . \tag{34}$$

Equation (33) can be rewritten to show that the energy per unit mass per unit volume scales according to $(\ell/\ell_o)^{2/3}$ by noting that

$$E_0 = (\bar{\varepsilon}\ell_0)^{2/3} \tag{35}$$

Then,

$$E_n \sim (\bar{\varepsilon}\ell_n)^{\frac{2}{3}} = (\bar{\varepsilon}\ell_0)^{\frac{2}{3}} (\ell_n/\ell_0)^{\frac{2}{3}} \sim E_0 (\ell_n/\ell_0)^{\frac{2}{3}} \quad , \tag{36}$$

There is a tacit (but very important) assumption in the above relationship: All eddy sizes are assumed to be spread more or less uniformly throughout the same volume. For greater

generality, Frisch et al. (1978) assumed that the smaller eddies are less space-filling than the larger ones. The behavior of free shear layer turbulence described in the preceding section qualitatively supports this assumption. Frisch et al. (1978) define a parameter to characterize the degree of space-fillingness. For a wholly space-filling cascade of the type discussed above, the number of eddies of size $\ell_n = \ell_0/2^n$ is 2^3 times as those of size ℓ_{n+1} because eight eddies of dimension $\ell/2$ fill the volume occupied by one of dimension ℓ. Frisch et al. (1978) defined β to be the average fraction of the ℓ_n volume filled by ℓ_{n+1} eddies. Eddies of size ℓ_n fill only a fraction, β_n, of the total space occupied by eddies of size ℓ_0:

$$\beta_n = (N/2^3)^n \quad , \tag{37}$$

where N is the average number of eddies formed by each eddy of the preceding generation, and of course $N \leq 8$.

Frisch et al. (1978) assumed that eddies of the $(n+1)^{th}$ generation are positionally correlated with those of the n^{th} generation by embedding or attachment, so that the region near where an eddy is formed becomes an "active region" for the cascade to smaller sizes. The evidence from mixing-layer turbulence suggests that attachment is more likely than embedding. Frisch et al. (1978) also tacitly assumed that the average number of eddies formed (N) does not vary systematically according to eddy size. This is a weakness of this "β model" of turbulence.

If the kinetic energy per unit mass associated with scales on the order of ℓ_n is redefined in terms of active regions only, then

$$E_n \sim \beta_n v_n^2 \sim \left(\frac{N}{2^3}\right)^n v_n^2 \quad . \tag{38}$$

The characteristic energy transfer time is still ℓ_n/v_n if the smaller eddies arise from the internal dynamics of the larger eddies that produce them, but the steady-state assumption leads to an adjusted rate of energy transfer in the inertial range; that is,

$$\varepsilon_n \sim \frac{E_n}{t_n} \sim \frac{\beta_n v_n^3}{\ell_n} \sim \bar{\varepsilon} \quad . \tag{39}$$

The following relationships are obtained from Eq. (39) when we introduce D, defined by $N = 2^D$:

$$v_n \sim (\bar{\varepsilon}\ell_n)^{1/3} (\ell_n/\ell_0)^{-(3-D)/3} \tag{40}$$

$$E_n \sim (\bar{\varepsilon}\ell_n)^{2/3} (\ell_n/\ell_0)^{(3-D)/3} \quad , \tag{41}$$

and

$$E(k) \sim (\bar{\varepsilon})^{2/3} k^{-5/3} (k \ell_0)^{-(3-D)/3} \quad , \tag{42}$$

Rewriting Eq. (42) shows the scaling nature of the relationships:

$$E_n \sim (\bar{\varepsilon} \ell_n)^{2/3} (\ell_n / \ell_0)^{(3-D)/3} = (\bar{\varepsilon} \ell_0)^{2/3} (\ell_n / \ell_0)^{(\frac{5}{3} - \frac{D}{3})} \sim E_0 (\ell_n / \ell_0)^{(\frac{5}{3} - \frac{D}{3})} \quad . \tag{43}$$

This is the same as Eq. (37), but with a correction of D/3 in the exponent to account for the incompleteness of space-filling (intermittency) in the energy transfer to smaller scales. The relationship among N, β, and D is

$$\beta = (N/2^3)^n = (2^{D-3})^n \quad . \tag{44}$$

The above derivation demonstrates the scaling properties of important turbulent parameters. It relates to classical theory and observed physical factors that cause intermittency. The fractal dimension was introduced as a measure of the assumed space-filling properties of the energy transfer process. When the process is assumed to be space-filling, the fractal dimension is 3, giving the classical results of Kolmogorov.

Fujisaka and Mori (1979) estimated values for D under the assumption that informational entropy would be maximized. Their analysis led to an estimate of D = 2.659 which is in good agreement with estimates based on observations. It also suggests that on average, there are 6.32 eddies of size ℓ_{n+1} for each eddy of size ℓ_n in the above analysis.

3. Numerical Simulation of Small-Scale Flow Structures

Most fluid flow simulations parameterize turbulent effects and so provide little evidence of fractal structures. However, Chorin (1982), using vortex methods like those described by Leonard (1985), performed an interesting numerical experiment that bears a close relationship to the formation of vortices in the braids between eddies. He considered a straight vortex with a single perturbation, much like one of the perturbations on the vortex filaments in braids between vortices. After a short while, the vortex tube segments stretched rapidly. The general orientation of the pattern remained the same, but it became contorted and complex. Chorin (1982) evaluated the Hausdorff dimension of the resulting structure and found it to be on the order of 2.5, which is consistent with values suggested by Mandelbrot (1977) for the fractal dimension of turbulent structures.

III IMPORTANT RESULTS

A. SUMMARY OF PROJECT ACCOMPLISHMENTS

The research conducted during this project has provided the following:

- A coherent review and summary of fractal concepts and their relevance to atmospheric behavior, especially as they apply to the turbulent dispersal of aerosols and gasses.
- Identification of several analysis techniques based on fractal concepts that can be applied to atmospheric data.
- Computer programs for calculating parameters necessary to estimate fractal dimension by methods described in the literature.
- Extension of the multiresolution feature analysis concepts to three-dimensional scalar and vector fields.
- Development of computer codes for applying the extended analysis techniques.
- Identification and acquisition of atmospheric data for analysis.
- Analysis of some of the available data.
- Development of a methodology (including computer programs) for identifying natural patterns of variability in scalar and vector fields, so that those patterns can serve as the basis for multiresolution feature analysis.
- Identification of promising approaches for future research.

The remainder of this section, and the concluding sections provide examples of these accomplishments.

B. IDENTIFICATION OF DATA SUITABLE FOR ANALYSIS

1. Background

The most important purpose of this study has been to examine the spatial inhomogeneities in plumes released in the atmosphere. Obviously, detailed observations of such plumes will provide the best possible data for analysis. It was possible to obtain two such types of data: One data set was collected with a airborne laser radar (lidar) to provide vertical planar cross sections of aerosol backscatter from an elevated power plant plume, and the other data set (only identified and obtained near the end of the study) consists of two-dimensional arrays of infrared transmittance measurements through a smoke plume released at the surface.

Another set of similar "data" was also analyzed. In this case, the data were calculated to have known fractal properties. While such data will never substitute for actual observations, they

have the important advantage of providing an image that can be used to test the performance of the analytical techniques that were applied to the observations. The generation of the test data also gave some insights into how one might go about generating artificial distributions for simulating the appearance and the effects of inhomogeneous smoke plumes on Army operations.

Another type of data was obtained for analysis, although they were not directly related to inhomogeneities in smoke plumes. Data obtained by dual Doppler radar observations of the motions of chaff in a convective atmospheric boundary layer provide a detailed picture of those atmospheric motions that are the ultimate source of the inhomogeneities in the distributions of interest. Analyses of these data have not proceeded as far as those of the scalars, in part because they are not as directly relevant to project objectives as are the smoke-plume observations.

All the data sources are discussed briefly below. That discussion is followed by a summary of the analyses that were completed.

2. Scalar Data

a. Random Brownian Fractal Test Data

Jones et al. (1991) and Saupe (1988) describe a method for generating spatial distributions of known fractal dimension by using the spectral relationships discussed earlier [Eqs. (5) and (10)]. The method is well-described in both the sources cited above; Saupe (1988) outlines the algorithm in a section of computer pseudocode. The description that follows is based on that given by Jones et al. (1991).

The process begins by generating a random array of complex numbers. The real and imaginary parts each have zero mean and unit variance. The examples shown in Figure 4, are based on a 256×256 array. The complex numbers in the Fourier plane are then multiplied by their distance from the origin (in wave numbers) raised to a power that ultimately determines the fractal dimension of the distribution to be produced. If f_1 and f_2 are the coordinates of a point in the Fourier plane and we wish to produce a real number array whose two-dimensional spectral density S scales with an exponent between 0 and 1, i.e.,

$$S(f_1, f_2) \sim (f_1^2 + f_2^2)^{-\gamma} \quad , \tag{45}$$

then the complex numbers in the random array multiplied by the following factor, $F(f_1,f_2)$:

$$F(f_1, f_2) = (f_1^2 + f_2^2)^{-\gamma/2} \quad , \tag{46}$$

where from [Eqs. (6) and (10)] we get the following expression for the resulting fractal dimension:

$$D = (3E + 2 - \gamma)/2 \quad , \tag{47}$$

or for $E = 2$, we can choose γ according to the following expression to obtain the desired fractal dimension:

$$\gamma = 8 - 2D \quad . \tag{48}$$

After the complex numbers in the Fourier plane have been multiplied by the appropriate value of F, the inverse Fourier transform is applied to obtain a new array of complex numbers in linear space. The real parts of this array form an array with the desired fractal dimension, at least within the limits of the resolution. Obviously, there will be a high-wave-number cutoff imposed by the discrete nature of the grid.

Figure 4 shows three examples generated as described above. Standard FORTRAN Subroutines from Press et al. (1986) were used to generate the desired random numbers and perform the inverse fast Fourier transform. The figure displays the results as gray scale imagery with 256 gray levels. The fractal dimensions for the three panels of Figure 4 are, 2.3, 2.5, and 2.7. The same arrays used to generate Figure 4 are analyzed later by three different methods for calculating fractal dimensions.

b. Lidar Observations of Smoke Plumes

Uthe (1983) described the operations of the airborne lidar downwind of an Electric power plant plume in Kincaid, Illinois. Figure 5 is a schematic diagram of the operations. The aircraft flies at about 3 km above ground level, and the 1.06-μm laser is pulsed at a rate that corresponds to a distance of about 10 m between each vertical profile of aerosol backscatter. The pulse length and recorder operation provide a vertical resolution of about 3 m. The result is an array of values corresponding to aerosol backscatter with a spatial resolution of about 3 m (vertical) by 10 m (horizontal).

Typically, the data were collected in a vertical plane approximately normal to the plume and 10 to 15 km downwind of the source. The logarithm of backscatter was recorded with 8-bit (256 units) resolution. Before analysis, the data were converted to a relative linear scale. The originally recorded range of 0 to 255 corresponded to 16 dB. Hence, each unit corresponds to an increase of almost 1.5%. These data were converted to a linear scale before analysis. Range corrections did not account for the attenuation introduced by the relatively low aerosol concentrations in the plume. This, and the fact that aerosol backscatter is not directly proportional to concentration limit the uses of the lidar, except for the determination of geometric measures. The fractal analysis techniques deal with geometric features which should be relatively unaffected by the lidar's limitations in estimating aerosol concentration.

The rectangular nature of the data elements, with horizontal dimensions 3.3 × the vertical, may have an effect on the results. However, the atmosphere tends to horizontally stratified with more damped vertical motions and stronger vertical gradients, so the horizontally stretched shape of the data elements may be more appropriate than a square shape.

Figure 6 shows three cross sections through a smoke plume measured about 11 km downwind of the source between about 0800 and 0830 on 20 July 1980. Brighter regions indicate higher backscatter. An area of 144 × 144 elements has been selected from the original, larger data arrays. Two of the analytical approaches—spectral analysis and multiresolution feature analysis—are best applied with data arrays whose dimensions are a power of two. Therefore 128 × 128 arrays centered on the plume were extracted from the images shown in Figure 6. The box-counting approach benefits by having arrays whose dimensions are divisible by many numbers, so the full 144 × 144 cells were used for that analysis.

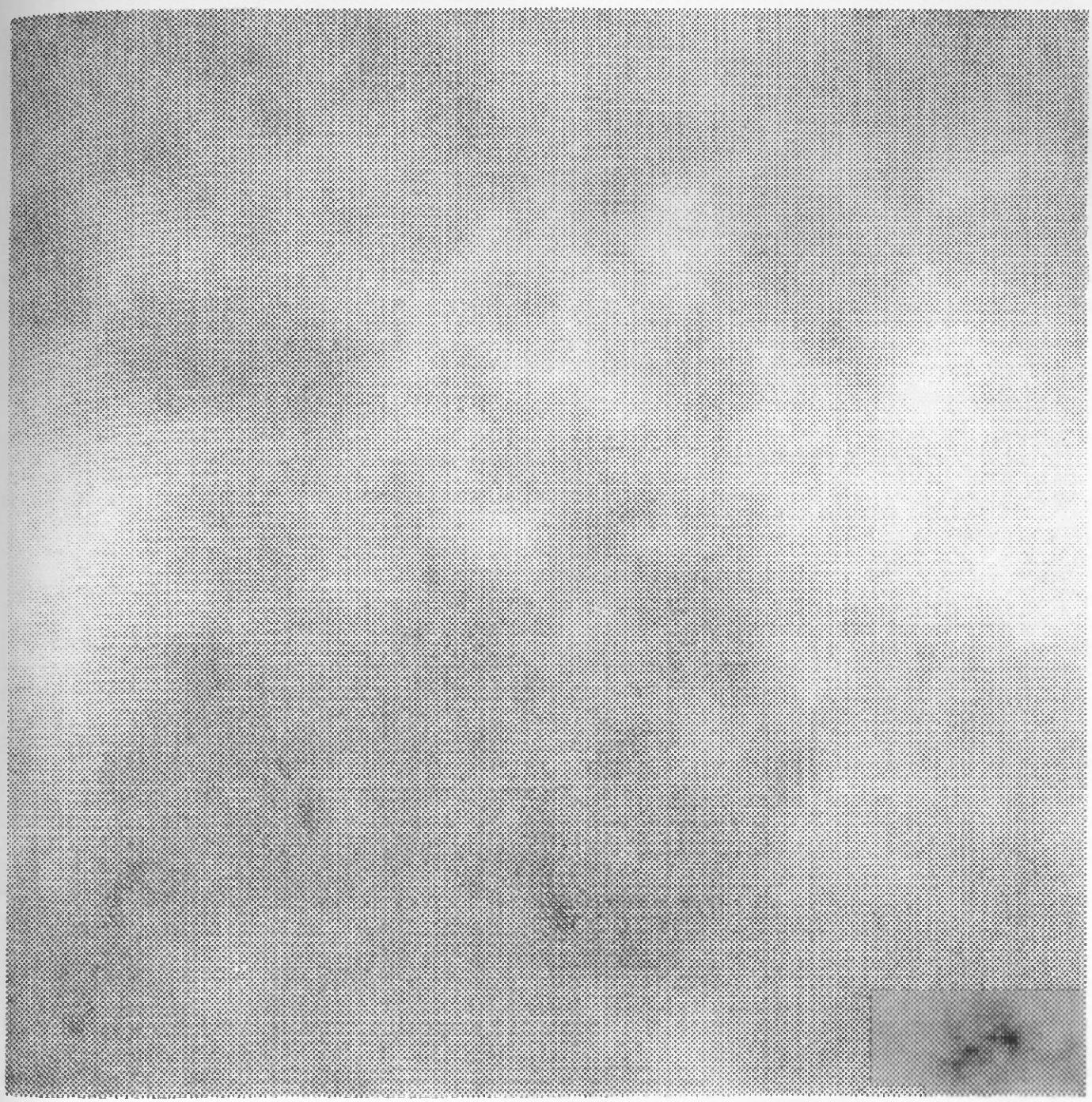

FIGURE 4 RANDOM BROWNIAN FRACTALS

(a) FRACTAL DIMENSION = 2.3

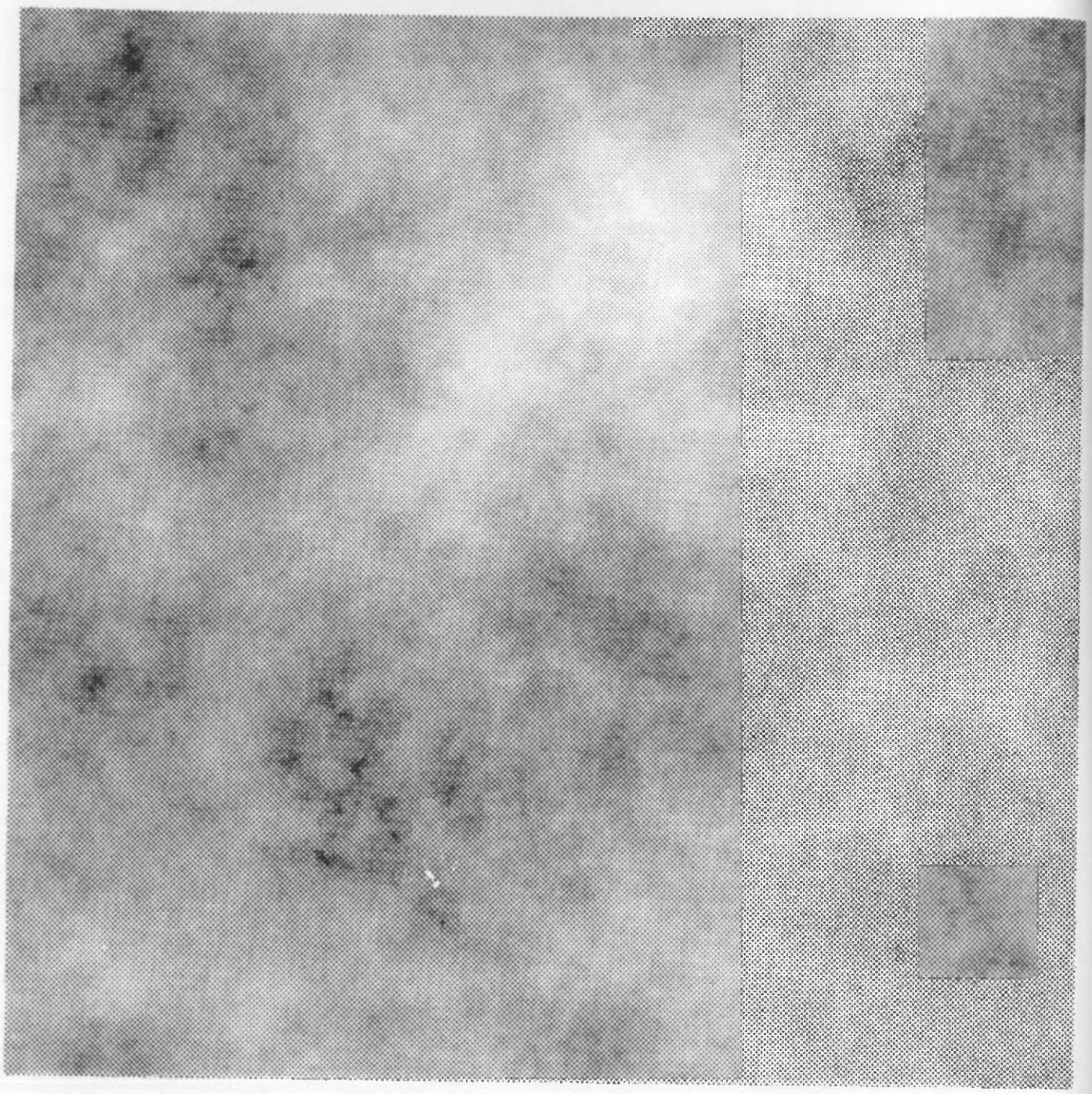

FIGURE 4 RANDOM BROWNIAN FRACTALS (continued)

(b) FRACTAL DIMENSION = 2.5

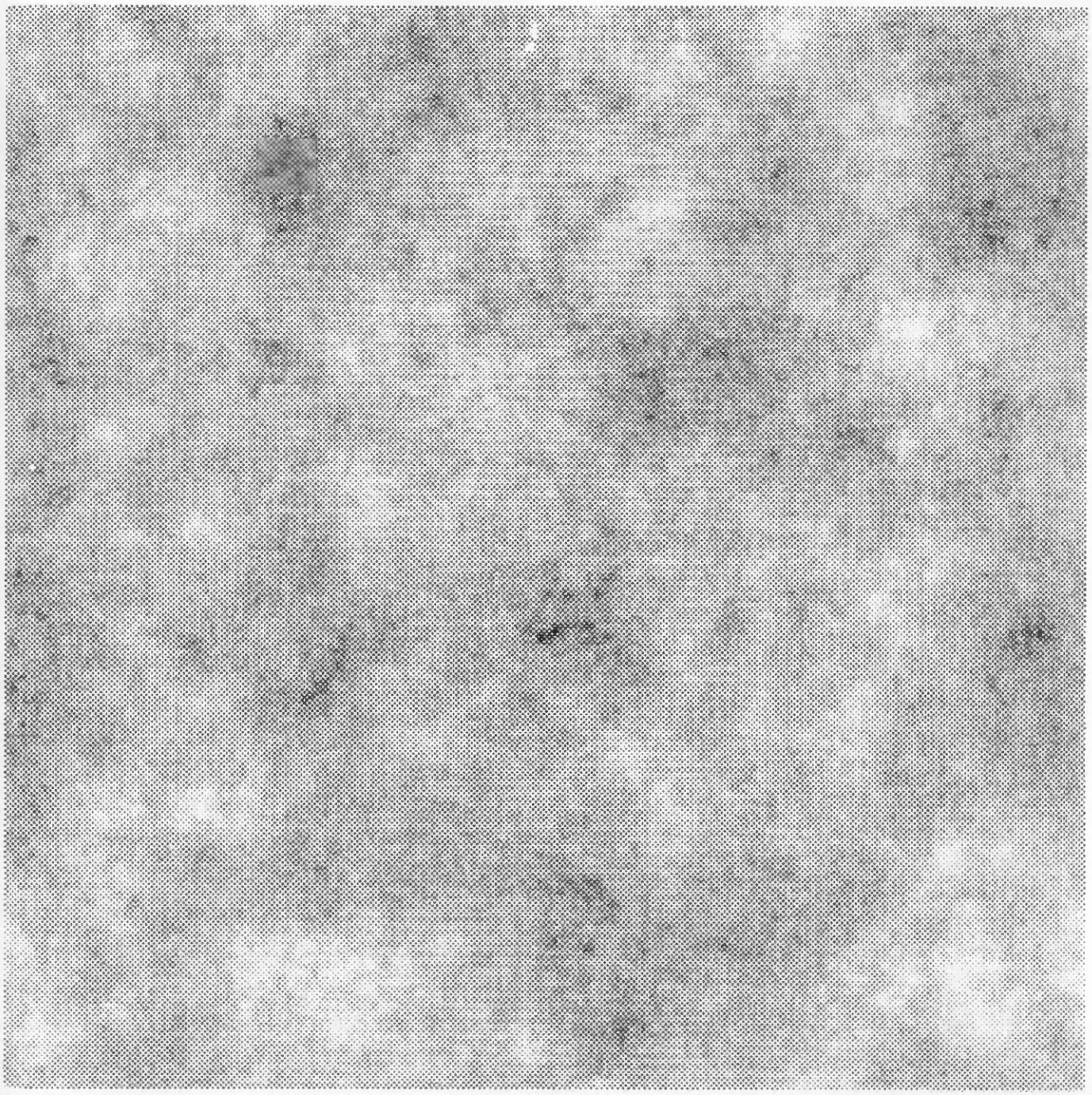

FIGURE 4 RANDOM BROWNIAN FRACTALS (concluded)

(c) FRACTAL DIMENSION = 2.7

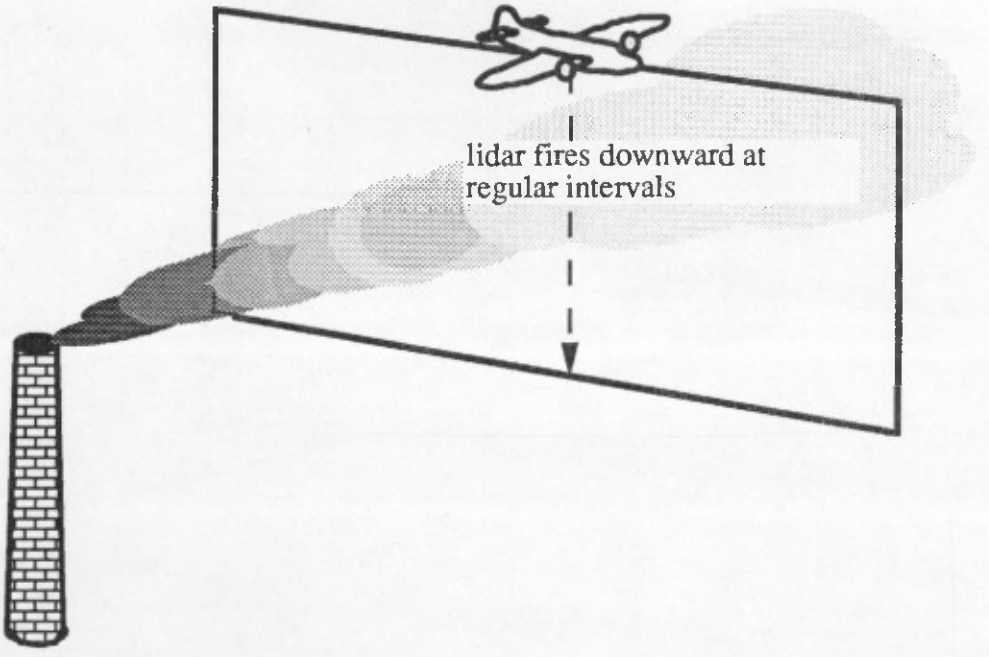

FIGURE 5 SCHEMATIC DIAGRAM OF LIDAR MEASUREMENT OF AEROSOL BACKSCATTER FROM A SMOKE PLUME

c. Transmissometer Images

The Atmospheric Transmission Large-area Analysis System (ATLAS), described by Bleiweiss et al. (1991), uses a video imaging system to generate two-dimensional arrays of transmittance values. The radiance of whatever is beyond the smoke plume being measured serves as the source for measurements. This means that several conditions must be met for the data to be reliable. First, the radiance of the background scene must remain constant during the measurement period. Second, there must be good contrast between the background radiance and that from a wholly opaque smoke plume. Unlike the lidar, backscatter data presented earlier (which depend on concentration), the ATLAS estimates transmittance from contrast observations. Transmittance depends on the integrated concentration along the line of sight.

Bleiweiss and his colleagues at White Sands Missile Range supplied 100 ATLAS transmittance images collected at 0.1-s intervals over a 10-s period. As noted by Bleiweiss et al. (1991) many assumptions are required. They assume single scattering and a spatially uniform medium so that transmission through the smoke T_c can be expressed in terms of source and cloud radiance L_s and L_c, and received radiance L_r as follows:

$$T_c = (L_r - L_c) / (L_s - L_c) \tag{50}$$

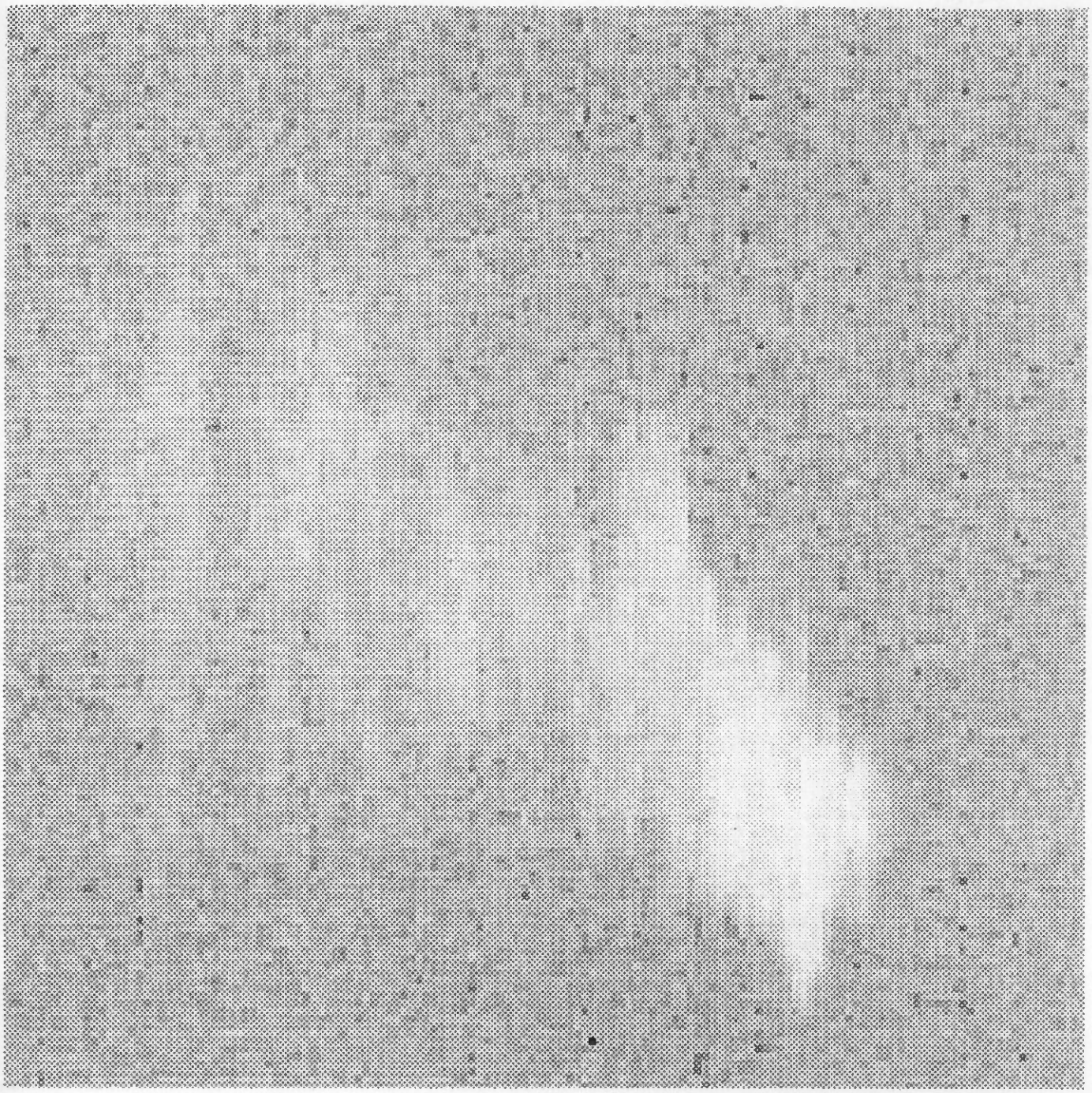

FIGURE 6 AEROSOL BACKSCATTER CROSS SECTIONS THROUGH A PLUME APPROXIMATELY 8 KM DOWNWIND OF THE KINCAID, ILLINOIS POWER—JULY 1980, APPROXIMATELY 0950 CST

(a) LIDAR CROSS SECTION 117

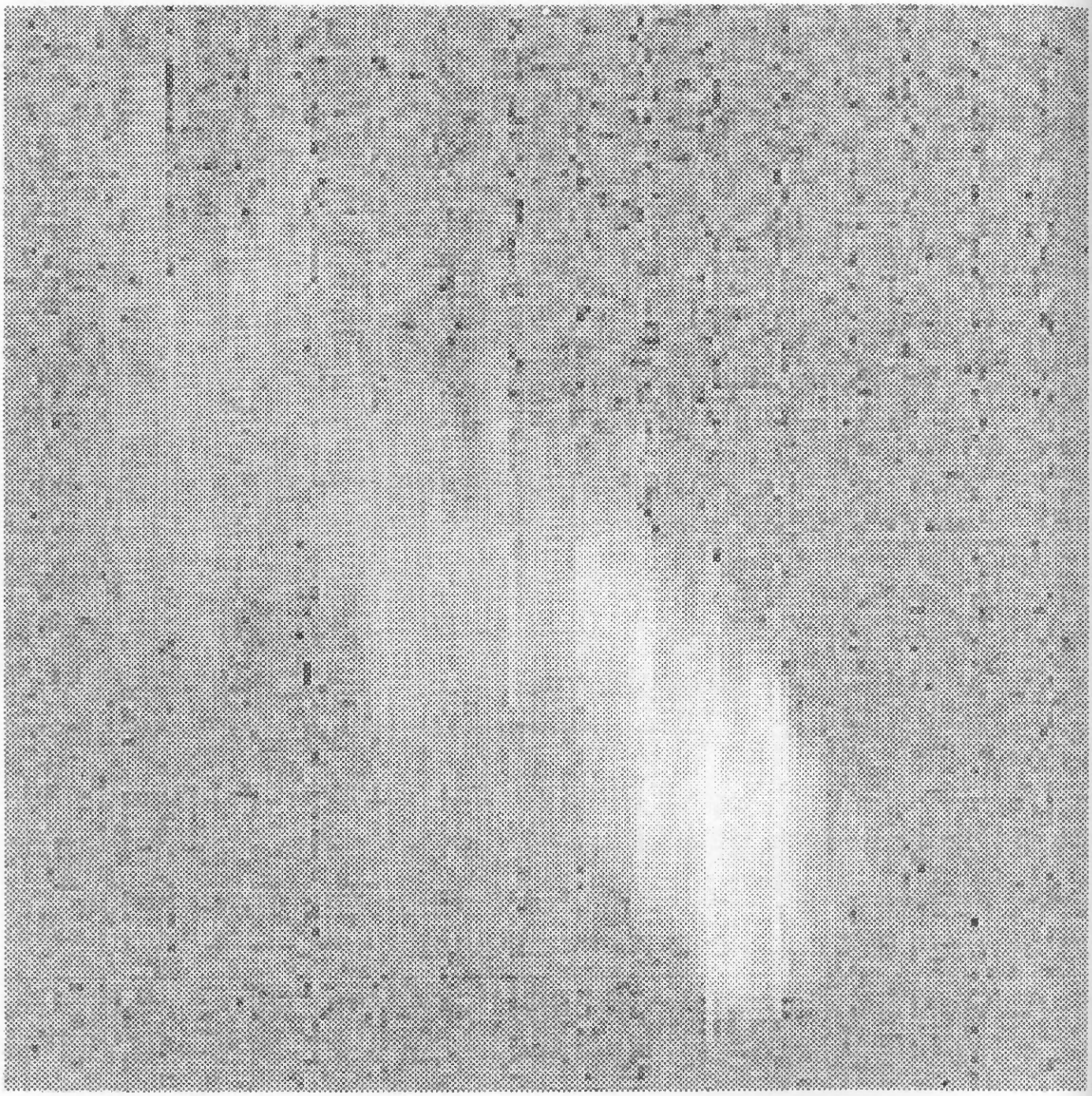

FIGURE 6 AEROSOL BACKSCATTER CROSS SECTIONS THROUGH A PLUME APPROXIMATELY 8 KM DOWNWIND OF THE KINCAID, ILLINOIS POWER—JULY 1980, APPROXIMATELY 0950 CST (continued)

(b) LIDAR CROSS SECTION 118

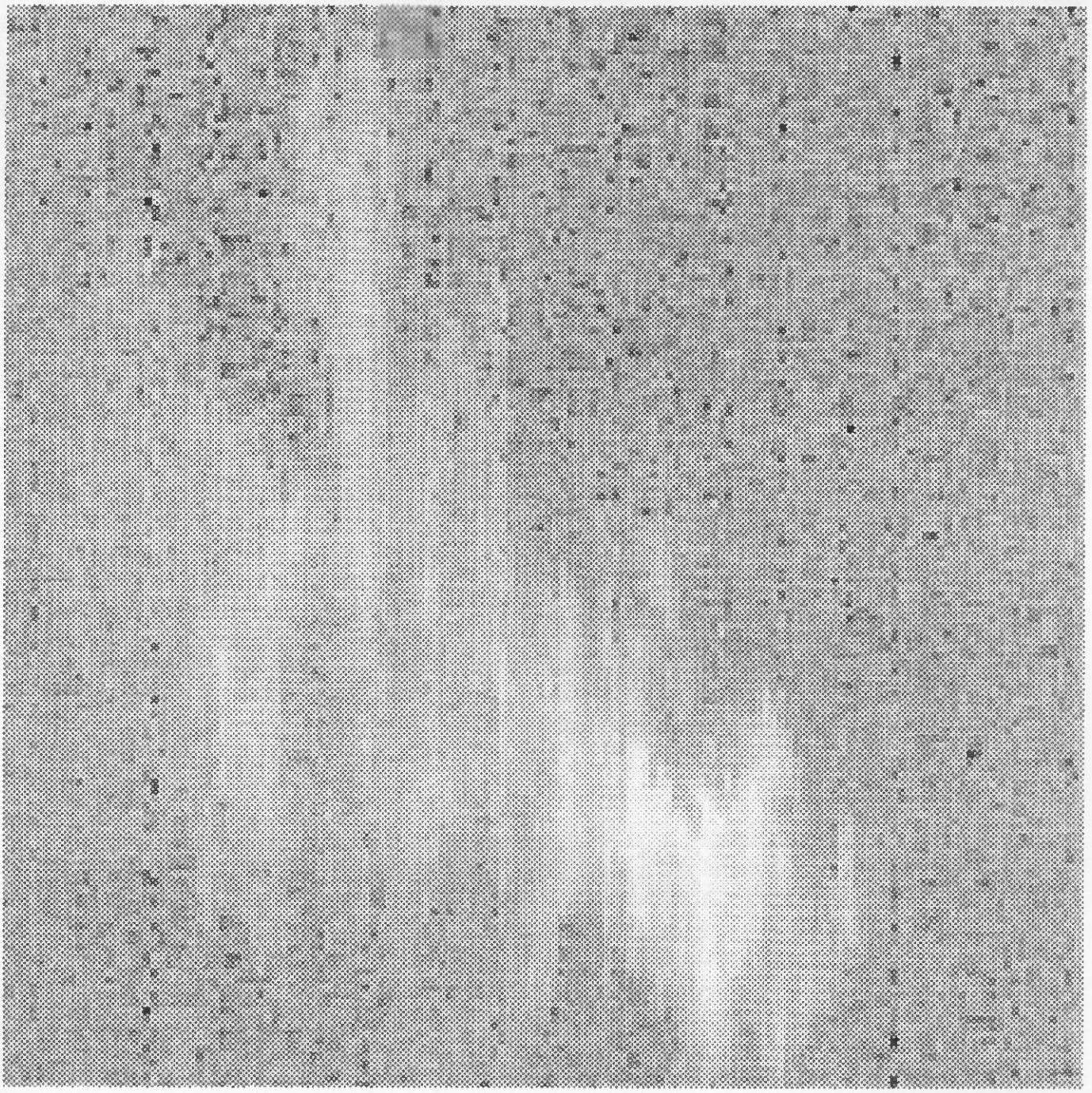

FIGURE 6 AEROSOL BACKSCATTER CROSS SECTIONS THROUGH A PLUME APPROXIMATELY 8 KM DOWNWIND OF THE KINCAID, ILLINOIS POWER—JULY 1980, APPROXIMATELY 0950 CST (concluded)

(c) LIDAR CROSS SECTION 119

Bleiweiss et al. (1991) assume that cloud transmittances T_c along nearby lines of sight with contrasting background radiance are equal and that there are no radiation sources off-line so that L_c can be estimated from the source and received radiances. If the two lines of sight and their corresponding background and received radiances are designated by subscripts 1 and 2, Eq. (50) can be rearranged to give

$$L_c = \frac{L_{S1}L_{R2} - L_{S2}L_{R1}}{(L_{S1} - L_{S2})(L_{R2} - L_{R1})} \tag{51}$$

Data presented by Bleiweiss et al. (1991) show that the ratio in Eq. (51) remains nearly constant during an experiment, thereby providing a means for estimating L_c, and from that the transmittance distribution. However, the data exhibit a strong peak in the horizontal wave number that corresponds to about three pixels (approximately 1 m). It is not clear whether this is an artifact of the data-reduction technique, but data at small spatial resolutions may not provide reliable results because of it.

Figure 7 shows three 128 × 128 pixel subsections of the transmittance images in the sequence supplied by Bleiweiss. Here, bright areas indicate higher transmittance, or less aerosol along the path. They correspond to times 1.5, 5.5, and 9.5 s from the beginning of the sequence. According to information supplied by Bleiweiss with the data, the "smoke" was an aluminum aerosol released from three generators about 500 m upwind from the part of the plume shown in Figure 7. The instrument was about 500 m from the plume. The measurements were made at 1831 EST, 16 May 1990 at Eglin Air Force Base, Florida. The winds at 10 m were about 4.4 ms^{-1} from the south. The atmosphere was neutral to slightly stable.

3. Vector Data

A unique set of atmospheric wind observations was made available to us by Schneider (1991). The data-measurement and reduction techniques are described in detail in the above cited reference. Very briefly these data were collected by observing the motions of small aluminum dipoles (chaff) with two Doppler radar systems separated by about 16 km. The two radars provided data from a volume about 9 × 9 km in the horizontal and 2 km in the vertical direction at a rate of about one complete volume measured every 2 min. The initial radial velocity measurements were interpolated to a Cartesian grid with 200-m spacing in all three directions. The grid is oriented with the Y direction toward north. The radial velocity data were smoothed to remove 400-m fluctuations. The data were also linearly interpolated to a common time between two successive volume scans. The u and v components are extracted from the two radial velocities at each grid point, first by ignoring the w component. The w component is then estimated from integration of the continuity equation and used to correct the first u and v estimates. Schneider (1991) found that the integration of the continuity equation gives more reliable estimates of w when performed in a coplanar, cylindrical coordinate system oriented along the radar baseline.

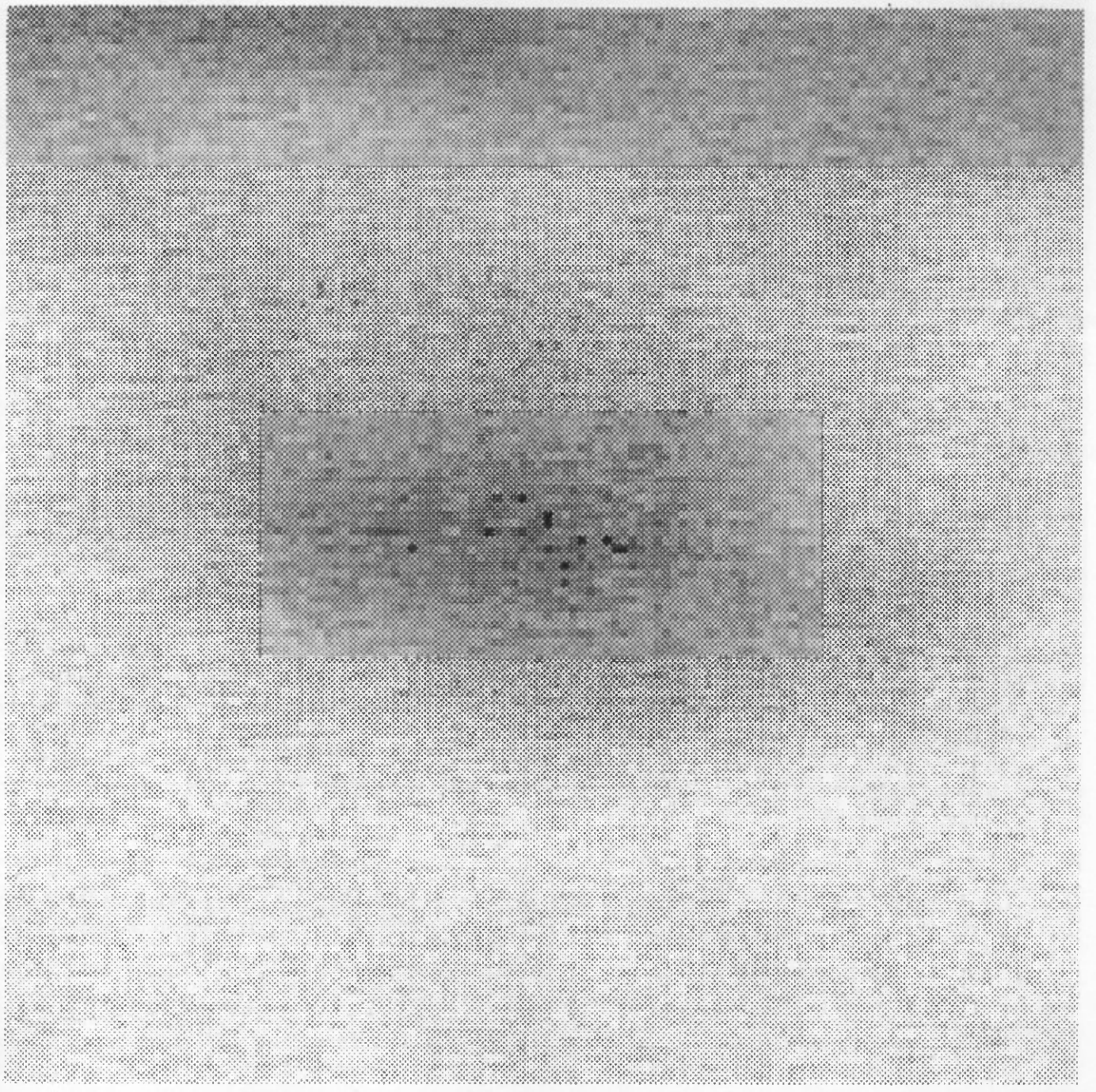

FIGURE 7 A SEQUENCE OF INFRARED TRANSMITTANCE IMAGES THROUGH AN ALUMINUM AEROSOL PLUME

Courtesy Bleiweiss et al., 1991

(a) 1.5 s

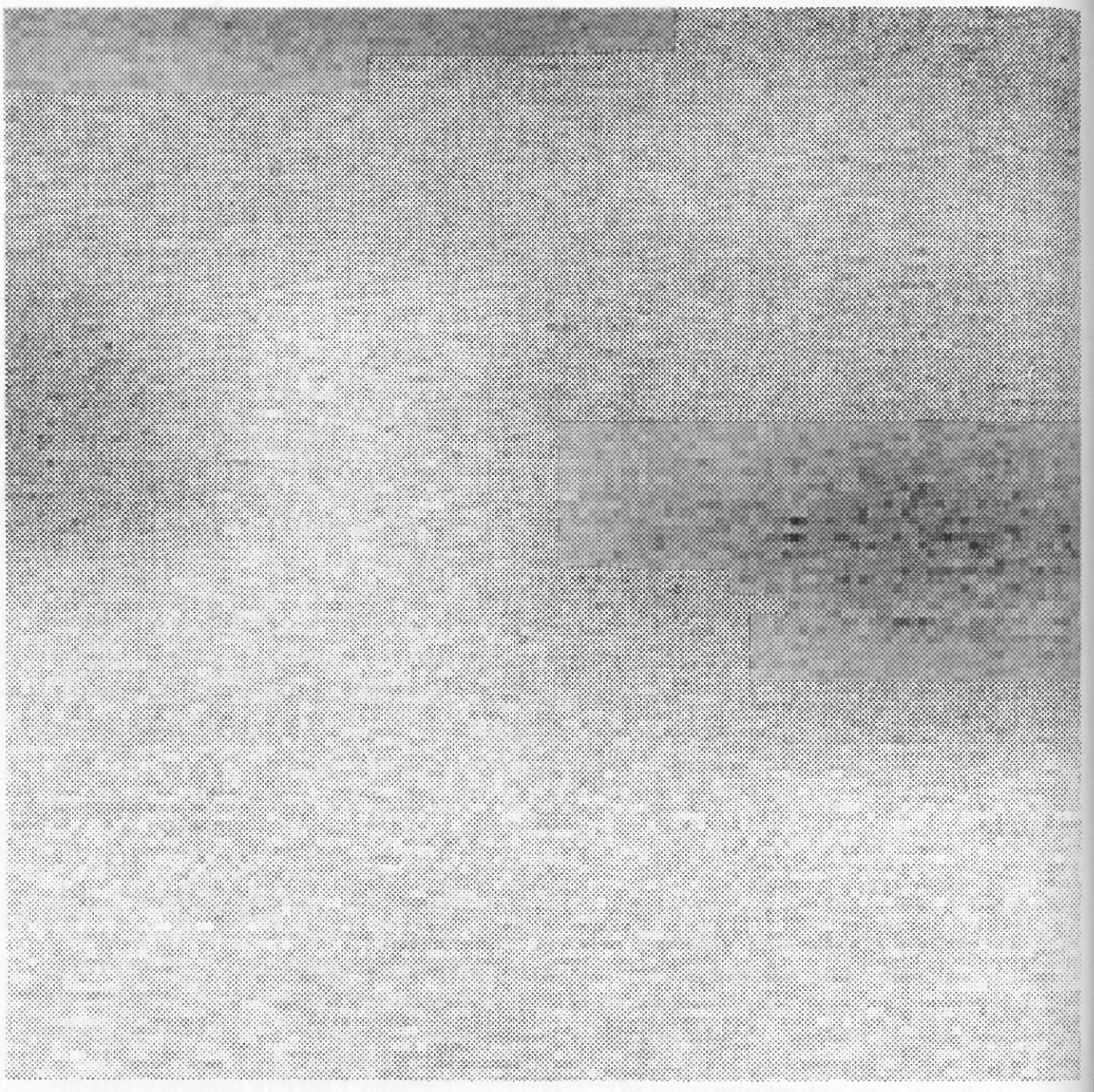

FIGURE 7 A SEQUENCE OF INFRARED TRANSMITTANCE IMAGES THROUGH AN ALUMINUM AEROSQL PLUME (continued)

Courtesy Bleiweiss et al., 1991

(b) 5.5 s

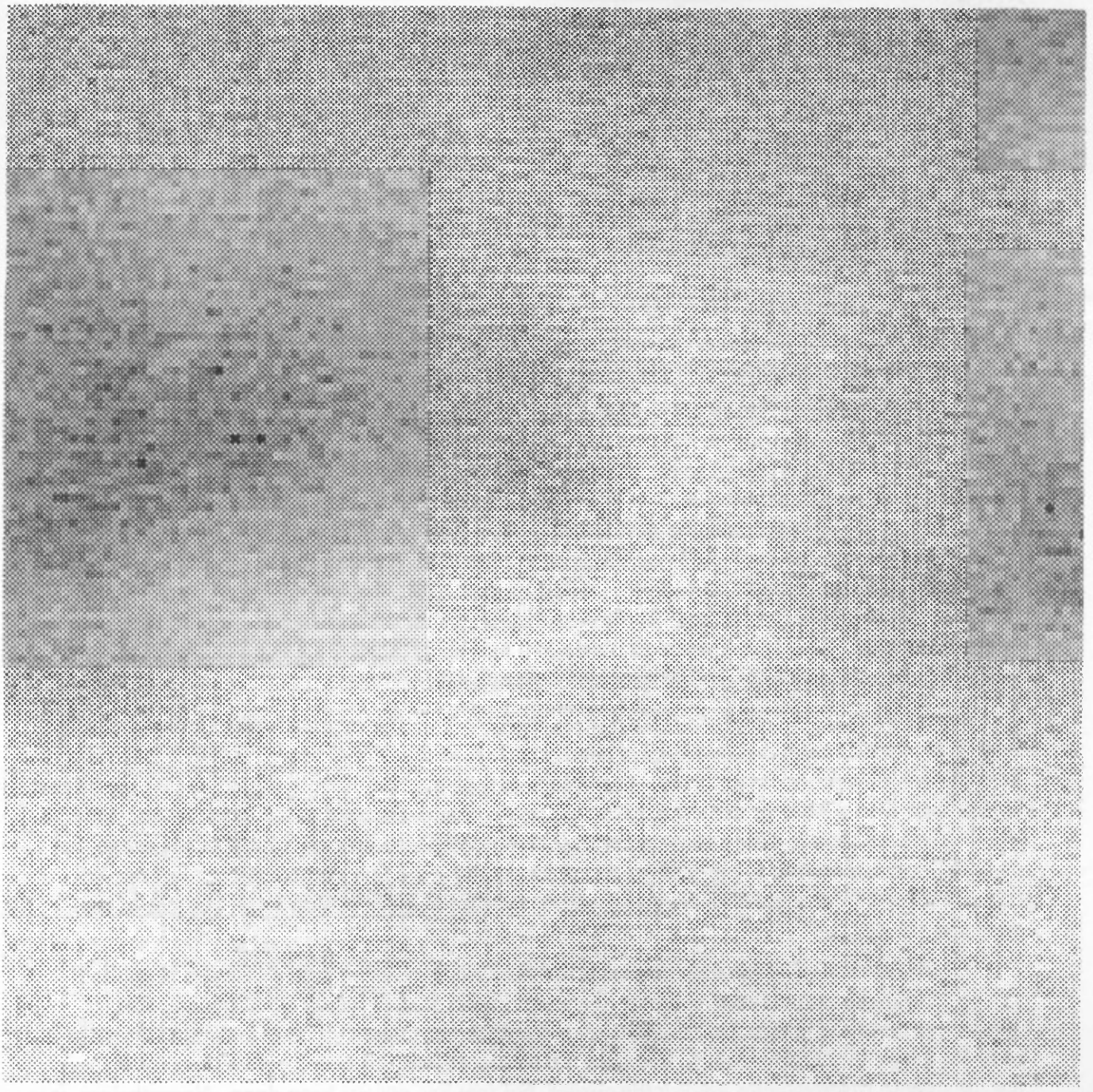

FIGURE 7 A SEQUENCE OF INFRARED TRANSMITTANCE IMAGES THROUGH AN ALUMINUM AEROSOL PLUME (concluded)

Courtesy Bleiweiss et al., 1991

(c) 9.5 s

The data provided by Schneider were in the form of the u, v, and w components at the grid points. It should be noted that the chaff tracked by the radar was not uniformly distributed so that there are some "holes" in the data. Furthermore, because the volumes scanned by the radars were such that there was no overlap in some corners, those grid points are also without data. Nevertheless, these data are complete enough that I began to consider applications to three-dimensional vector fields of the fractal dimension estimation methods discussed earlier. As of the writing of this report, we have not fully developed the necessary methodologies. The discussion of the dual Doppler wind data is included to demonstrate that there are data to which the methods described later can profitably be applied.

C. APPLICATIONS OF STANDARD FRACTAL ANALYSIS TECHNIQUES

1. Fourier-Synthesized Fractal Arrays

The data shown in Figure 4 were generated to demonstrate the degree to which the different fractal dimension estimation techniques can recover the "true" fractal dimension. In this case, the data are known to conform to the definition of a fractal, but (as we shall see) data collected in the atmosphere do not behave ideally. We would expect that, inasmuch as the test data were generated by Fourier synthesis, the Fourier methods for estimating fractal dimension would work well. This proves to be the case as can be seen in Figure 8. The three panels in Figure 8 show the power spectra (averaged according to radial distance from the origin in the Fourier plane). As expected, the slopes of the best-fit lines correspond to the correct fractal dimension within 2% in the worst case. This is indicative of the degree to which fractal dimension can be recovered under the best of circumstances for an array of this size (256^2).

Figure 9 shows the results obtained when the box-counting approach was applied to these same data. In this case, the data were treated as a three-dimensional array. A 240×240 subsection was taken from the larger array. The values at each grid point were scaled so that the largest values were also ≤ 240. In this case, lines with slopes corresponding to the exact fractal dimensions have been drawn. They show good agreement with the points over most of the range, but the points corresponding to the smaller sizes tend to show too few points. If best-fit lines are calculated for all but several of the upper points, the slopes agree within a few percent of the expected values.

Figure 10 shows the results obtained when the multiresolution figure analysis is applied using the four-orientation edge detector discussed earlier [see Eq (13)]. Without any formal quantification of the congruence of the curves for different thresholds, this technique does not have the sensitivity of the others. It should not be too difficult to develop a method for measuring the overall discrepancies among the curves, but that has not yet been done. Nevertheless, it is apparent that the center panel of each figure, which corresponds to the correct fractal dimension, has the most nearly coincident curves.

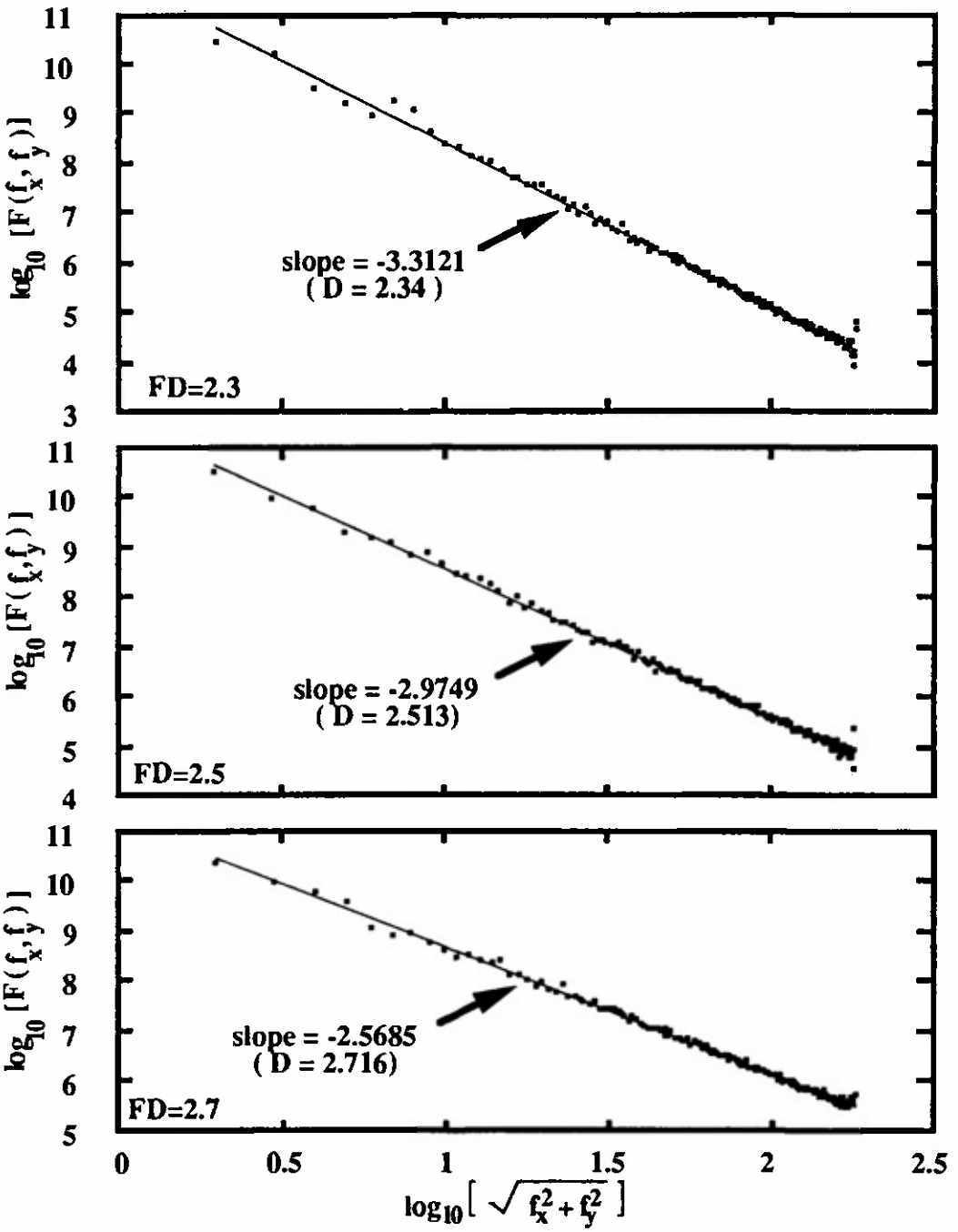

FIGURE 8 POWER SPECTRA FOR SYNTHESIZED BROWNIAN FRACTALS

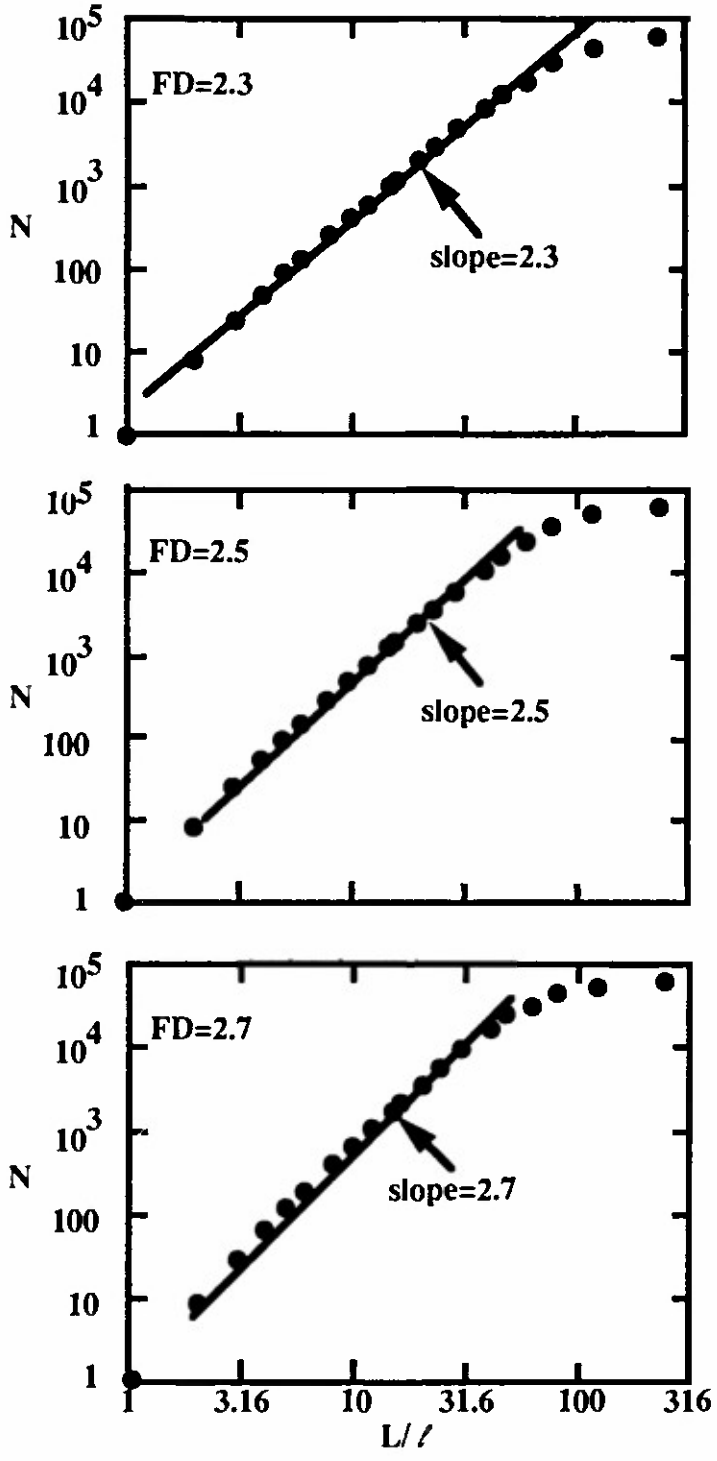

FIGURE 9 BOX-COUNTING ANALYSIS OF SYNTHESIZED BROWNIAN FRACTALS

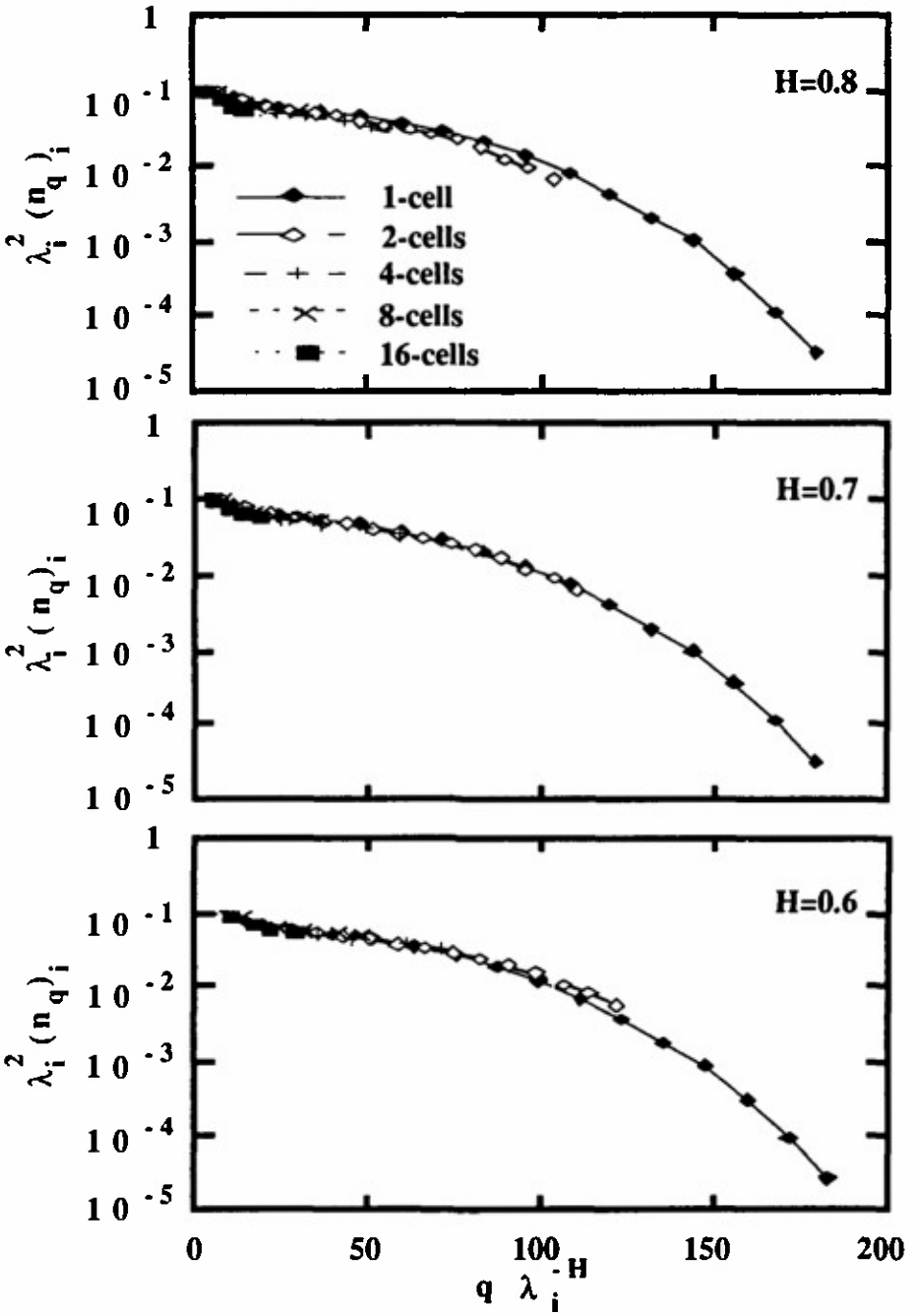

FIGURE 10 MULTIRESOLUTION FEATURE ANALYSIS OF SYNTHESIZED FRACTALS

(a) FRACTUAL DIMENSION 2.3

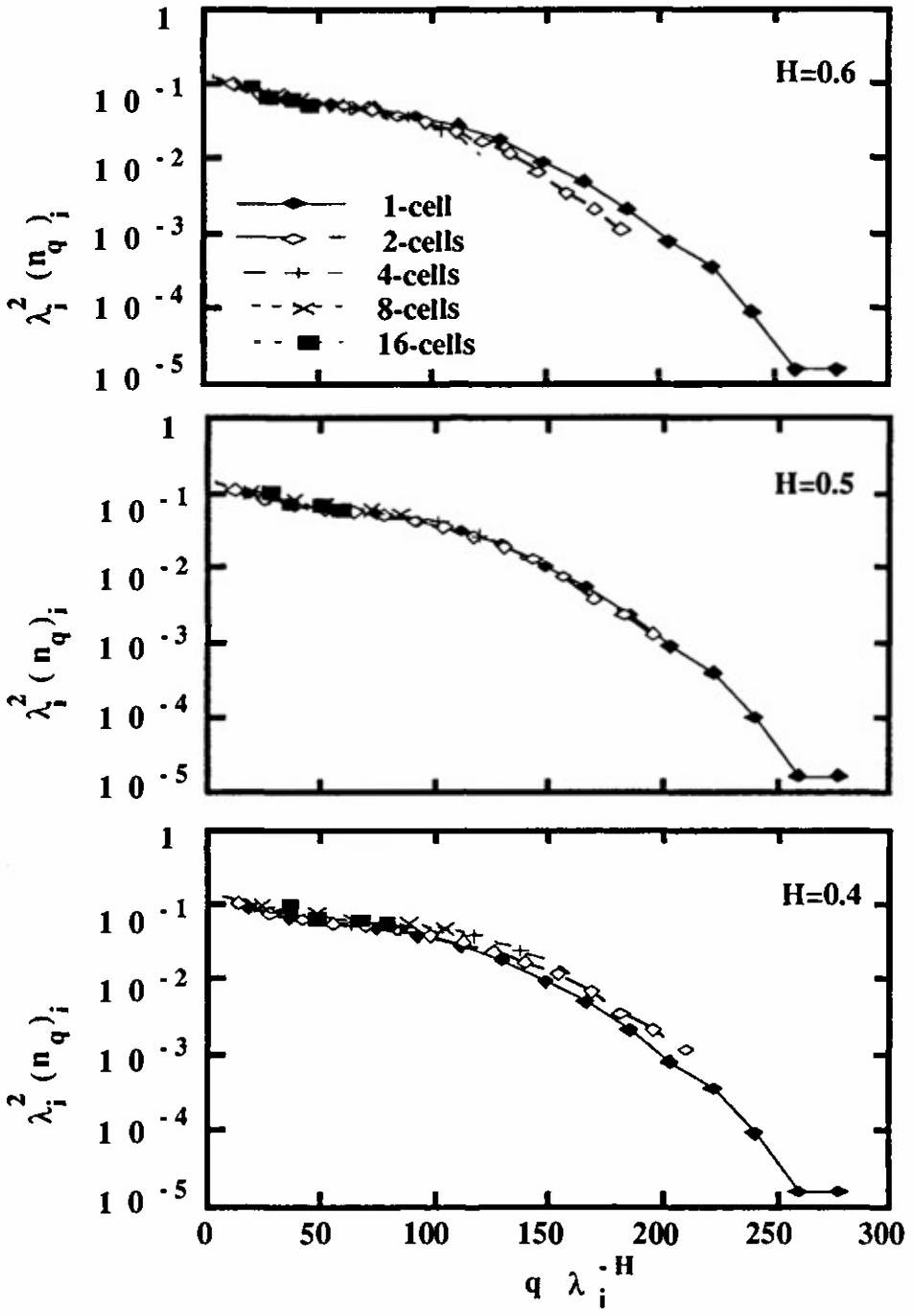

FIGURE 10 MULTIRESOLUTION FEATURE ANALYSIS OF SYNTHESIZED FRACTALS (continued)

(b) FRACTUAL DIMENSION 2.5

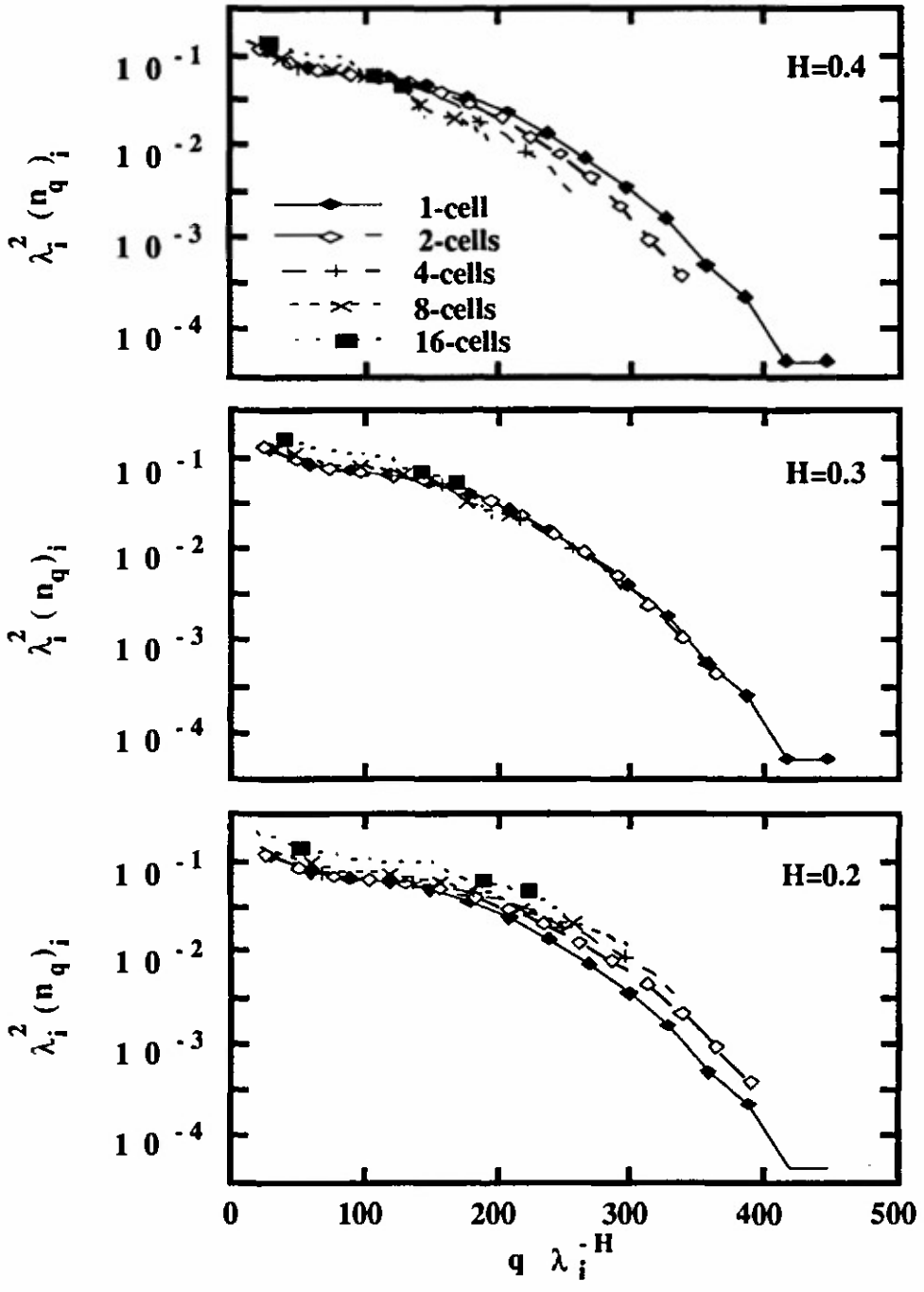

FIGURE 10 MULTIRESOLUTION FEATURE ANALYSIS OF SYNTHESIZED FRACTALS (concluded)

(c) FRACTUAL DIMENSION 2.7

2. Lidar Data

In principle, there is no reason why the same analysis techniques used in the preceding section cannot be applied to any two-dimensional array of numbers, such as those representing the lidar images of Figure 6. The presumption is that if the array has the properties associated with fractals, then that can be determined along with the fractal dimension. The presence of noise and errors in the data makes the problem more difficult. Figure 11 shows the power spectra obtained from the lidar images in Figure 6. Figure 11 also shows the best-fit straight lines and their slopes. The fractal dimensions inferred from these slopes are generally ≥ 3, which seems unrealistic. The box-counting estimates shown in Figure 12 suggest a value between 2.5 and 2.6, at least over the range of larger sizes where the straight lines fits are appropriate. Dashed straight lines of slope –2.9 (corresponding to a fractal dimension of 2.55) have been entered in Figure 11. It is apparent that they are in reasonable agreement with the box-counting results for the lower wave numbers (larger wavelengths). It is not certain whether the aerosol backscatter is not scaling over the entire range of sizes, or whether there is random noise in the data on a smaller scale. Data uncorrected for attentuation would be expected to have somewhat greater power at wave numbers associated with large-scale features (Uthe, 1991 personal communication). More recent data from improved lidar systems and correction for attenuation may resolve this question.

Figure 13(a) is an example of the application of the multidimensional feature-analysis technique to the lidar plume imagery. This figure is based on the occurrence of "edges" in the imagery. For purposes of comparison, Figure 13(b) shows a similar analysis of the same image, based on the occurrence of peaks [Eq. (14)]. In both cases, it is obvious that the fine resolution (one cell, or pixel) counts do not scale the same as the coarser features. This is certainly consistent with the findings from the spectral and box-counting analyses. It also appears that the two features—edges and boxes—have different scaling properties. Figure 13 shows the results for the three values of the exponent H that were judged to give the nearest congruence of the curves. Figure 13(a) suggests that the best estimate of fractal dimension derived from the edge analysis would be on the order of 2.6 or 2.7, reasonably consistent with the other methods. The peak analysis in Figure 13(b) gives an estimate nearer 2.9, considerably different from the other methods. Although the congruence of the graphs in the figures is poor, especially compared to the ideal cases shown in Figure 10, the fact that the two features give very different results suggests that the scaling properties may depend on the nature of the feature selected. This in turn suggests that appropriate features may not have been selected. This will be discussed further in a later section of this report.

3. Transmittance Imagery

Applications of the fractal analysis techniques were least successful for the transmittance imagery. This may be a result of the data-reduction techniques that were used. As noted earlier, there appears to be an artifact in the data that produces peaks in the horizontal spectrum at wavelengths on the order of a meter. Bleiweiss et al. (1991) discuss other data-reduction approaches in their paper that do not rely on the same assumptions. Future studies should compare results obtained from images using different data reduction methodologies.

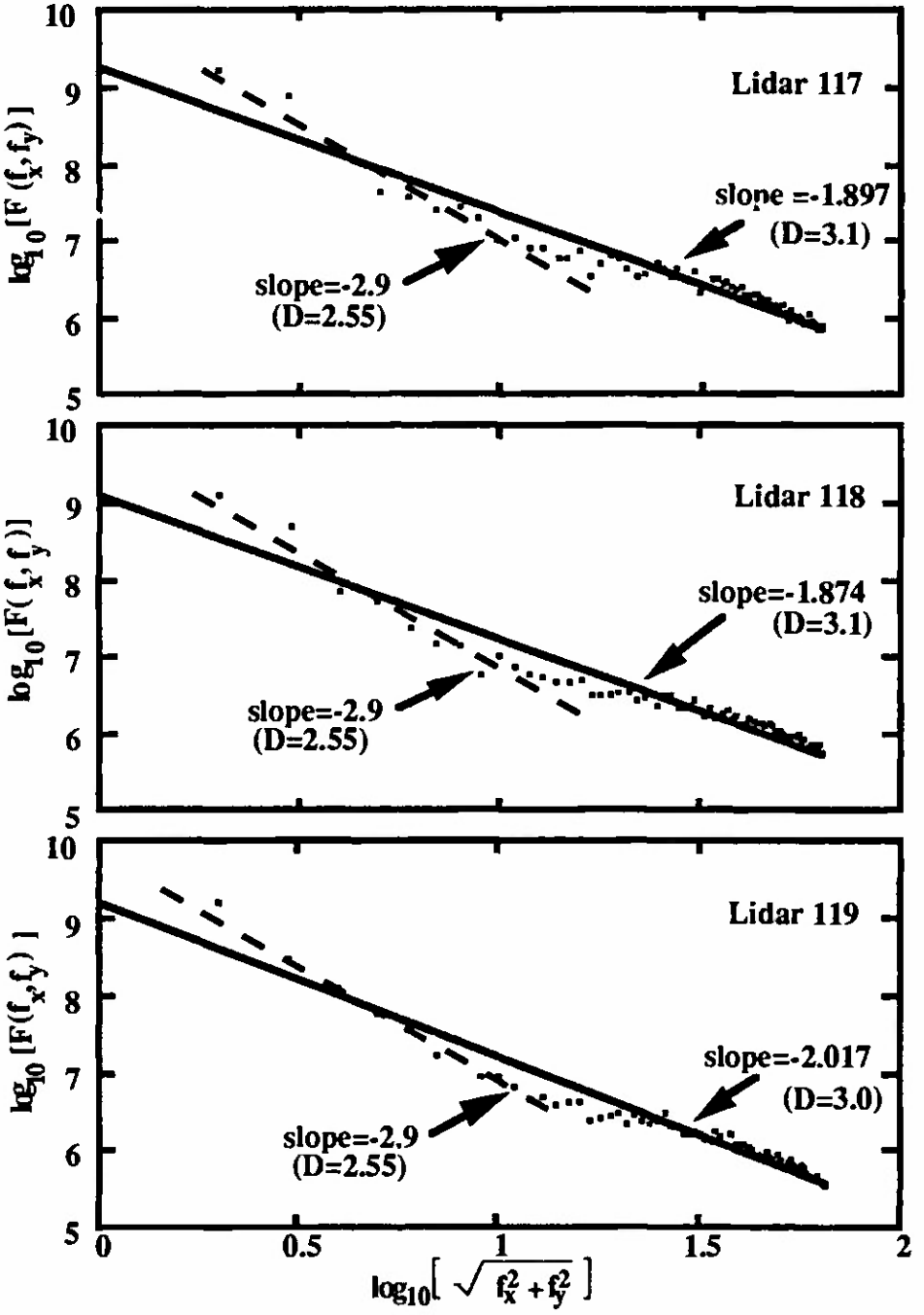

FIGURE 11 POWER SPECTRA FOR LIDAR PLUME IMAGES

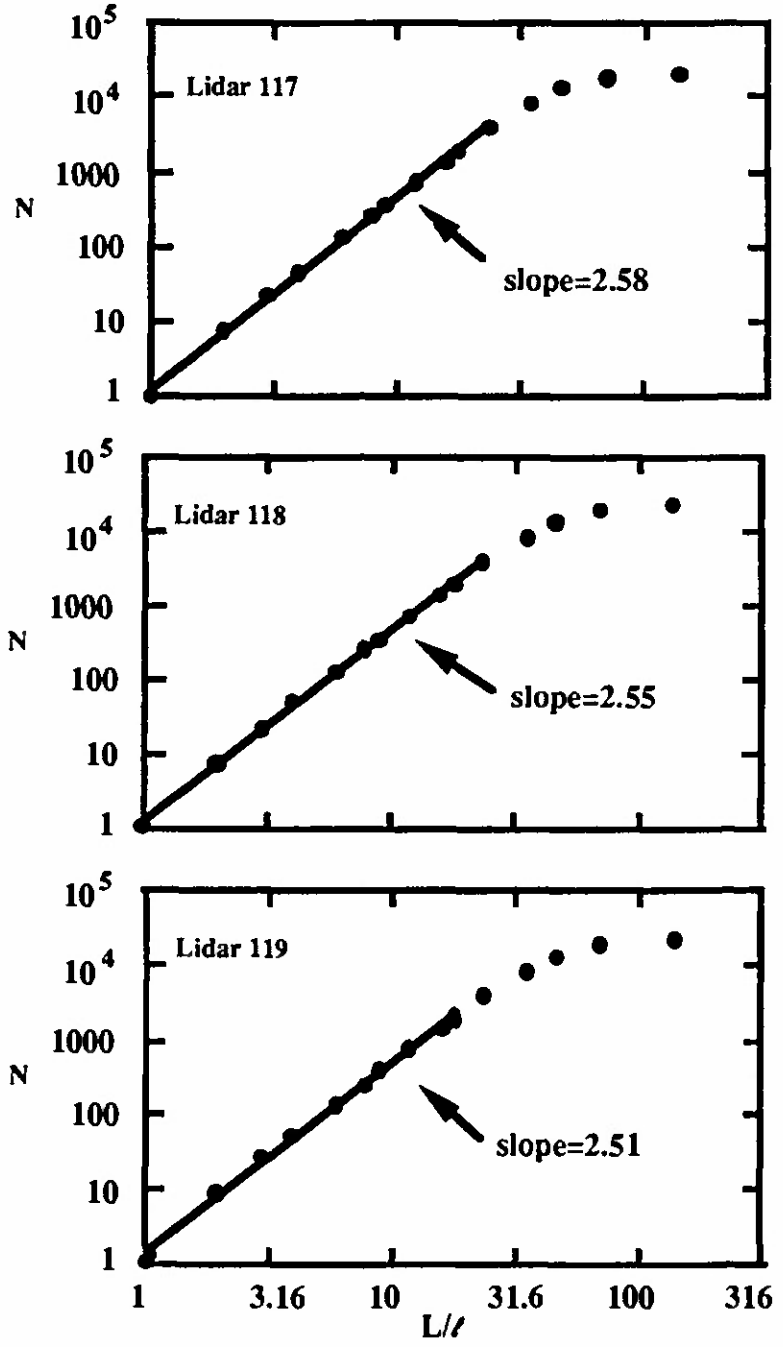

FIGURE 12 BOX-COUNTING ANALYSIS OF LIDAR PLUME IMAGES

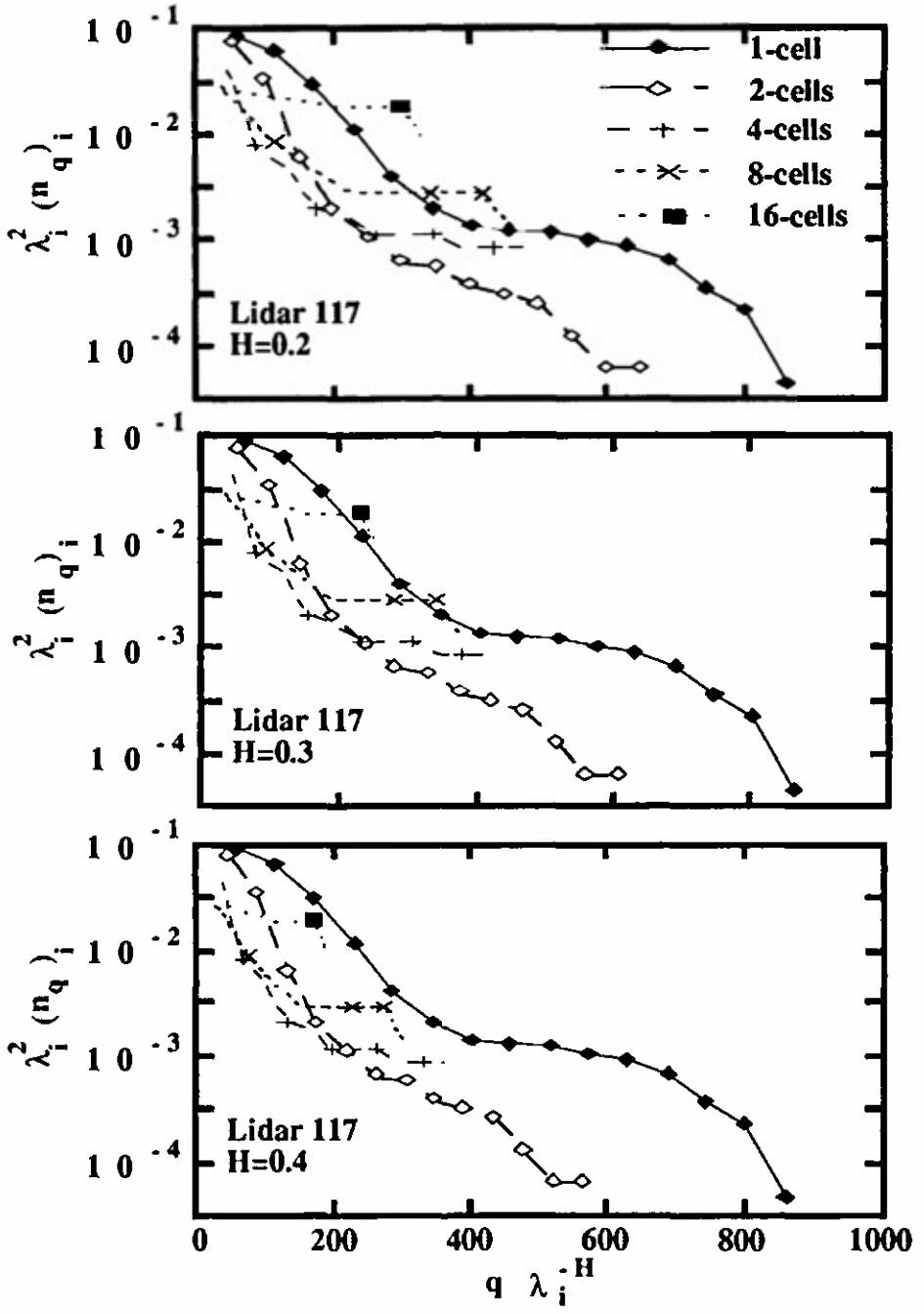

FIGURE 13 MULTIRESOLUTION ANALYSIS OF FIRST LIDAR PLUME IMAGE

(a) EDGE ANALYSIS

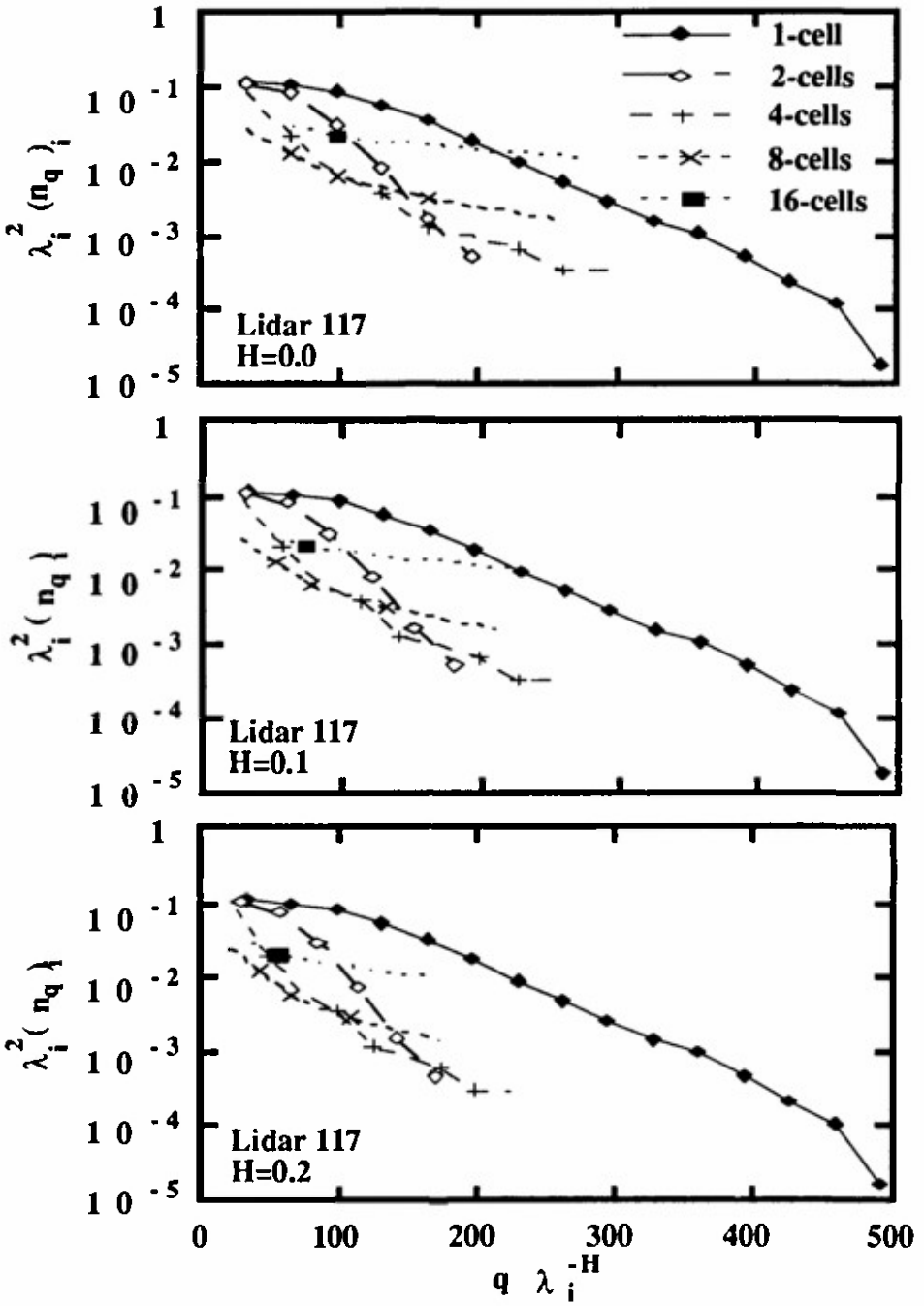

FIGURE 13 MULTIRESOLUTION ANALYSIS OF FIRST LIDAR PLUME IMAGE (concluded)

(b) PEAK ANALYSIS

In spite of problems with the data, some results were obtained. Figure 14 shows the power spectra for the three transmittance images in Figure 7. There is considerable variation among the images. It should also be noted that if the larger wave number (smaller wavelength) data points were ignored, the slope of the lines would be steeper, giving lower fractal dimensions. There is reasonably good agreement between the estimates of fractal dimension from the spectral slope and those from the box-counting method shown in Figure 15 for the first and last of the images. The other image is estimated to have a lower dimension from the spectral slope than from the box counting.

As with the lidar images, the transmittance images do not give very good results with the multidimensional feature-analysis approach. The origin of the problem is not clear. It may be the use of inappropriate features, or the data-reduction techniques mentioned earlier. Because the transmittance data are appropriate for the study of questions of considerable interest to the Army, every effort should be made in the future to use these data to determine the nature of inhomogeneities in the transmittance through smoke plumes.

D. EXTENSIONS OF MULTIRESOLUTION FEATURE ANALYSIS

1. Vectors

a. Two-Dimensional Fields

Scalar fields have been the focus of the discussion to this point, but multiresolution feature analysis can also be applied to vector fields. Two possible approaches exist:

- Apply any of the techniques to some scalar property of the vector field, such as divergence or the vertical component of vorticity.
- Define vector features and apply the multiresolution methodology directly to the vector field.

Some of the conventional finite-difference approximations for vector field properties can be represented by features like that represented in Figure 16. It shows the finite-difference operator for the vertical component of vorticity expressed as the sum of two features (like those presented earlier as matrices to be superimposed on the data field to define a sum of products): One of these "templates" is applied to the westerly (u) component, the other to the southerly (v) component. Ordinary scalar feature detectors can then be applied to the resulting feature intensity field, although the interpretation may not be straightforward. Figure 17 shows a flow field that would be associated with an "edge" in the vorticity field.

Scalar properties of the vector field need not be used; interpretation of the results may be much easier if vector features are defined and applied directly to the field. Figure 18 shows two particularly interesting vector features. The vector templates are applied in the same way as the scalar templates, except that the arithmetic product is replaced by the scalar (dot) product of each feature vector and the corresponding vector in the field being analyzed. If the vortex feature template in Figure 18(b) is applied to variously smoothed vector fields, then we are actually

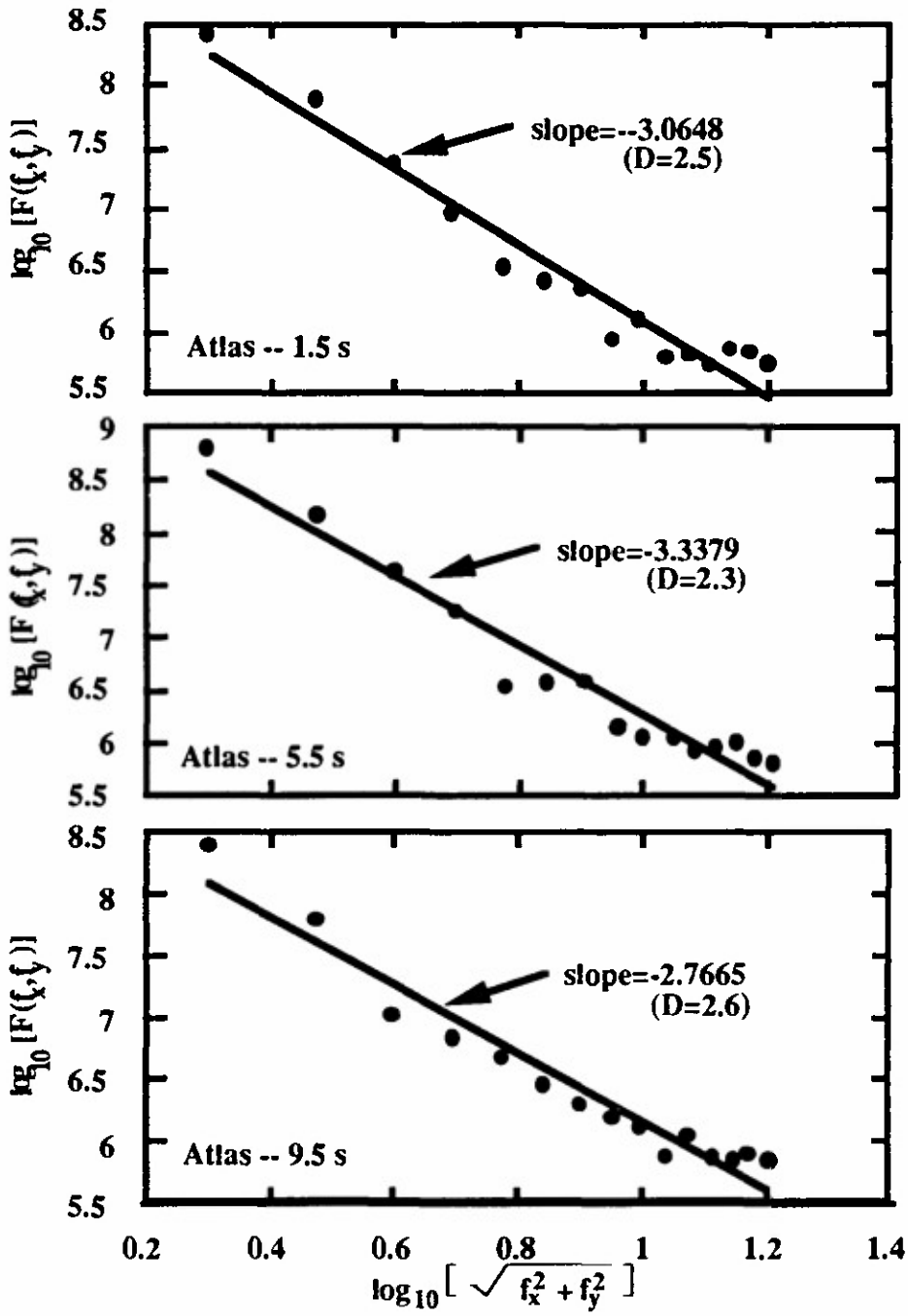

FIGURE 14 POWER SPECTRA FOR ATLAS TRANSMISSOMETER IMAGES

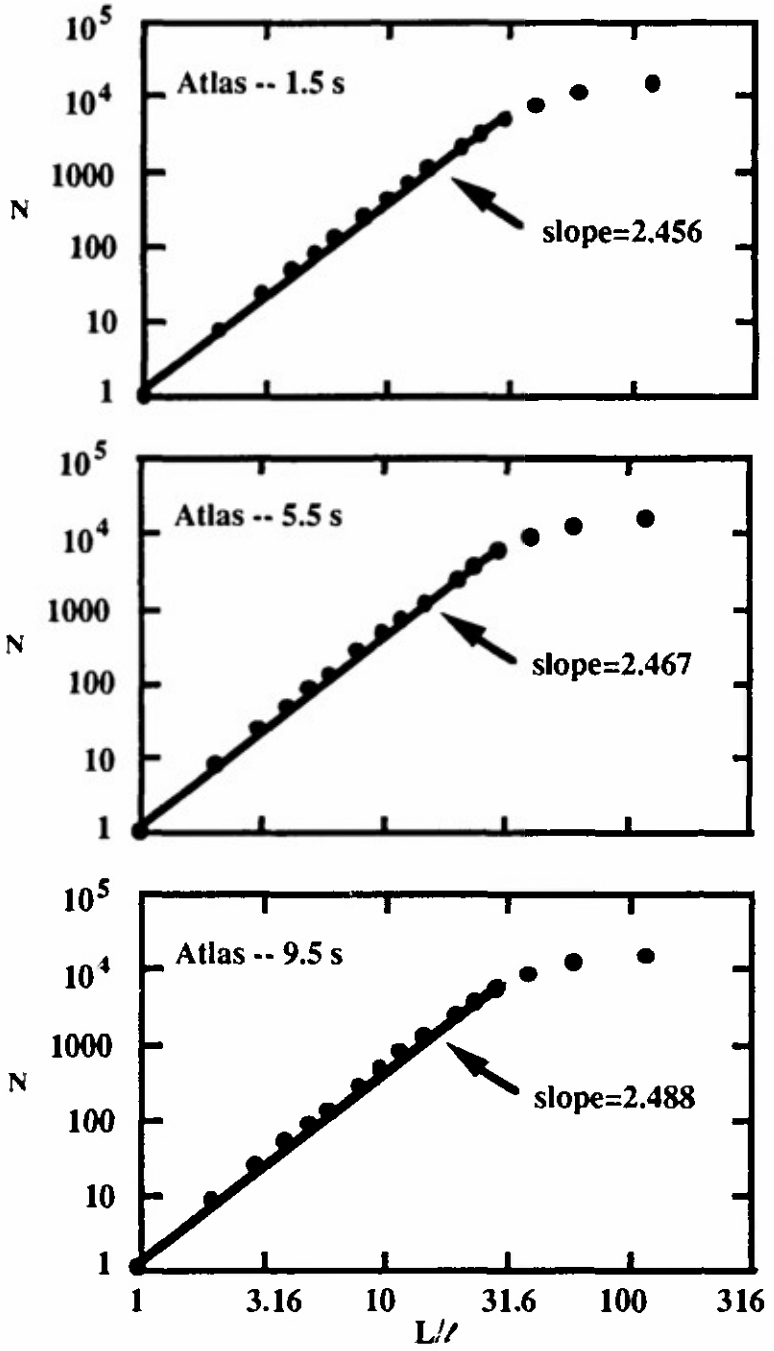

FIGURE 15 BOX-COUNTING ANALYSIS OF ATLAS TRANSMISSOMETER IMAGES

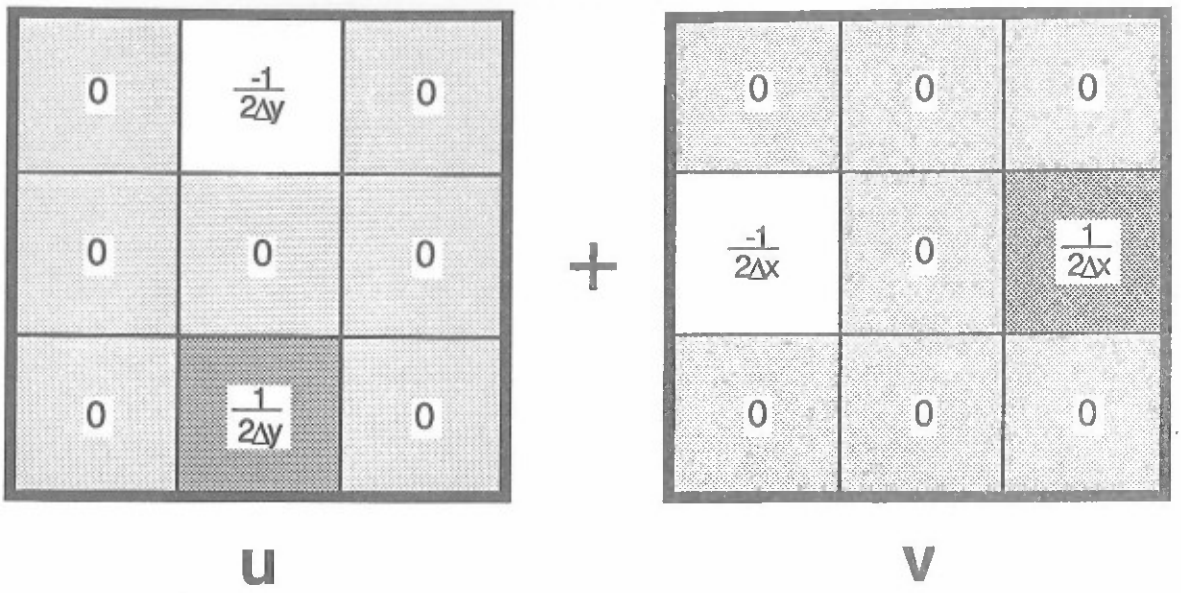

FIGURE 16 FEATURE BASED ON THE FINITE-DIFFERENCE APPROXIMATION FOR THE VERTICAL COMPONENT OF VORTICITY

pursuing the quantitative meaning of Richardson's doggerel that "Big whorls have little whorls..." (Richardson, 1922, as quoted by Mandelbrot, 1983). The whorls or vortices in Figure 18(b) are two-dimensional features, that might be associated with the feature in Figure 18(a) oriented in a perpendicular plane.

b. Three-Dimensional Fields

One of the mechanisms suggested for the transfer of energy down the turbulent cascade is by the stretching of vortex filaments. Figure 18(a) shows a flow pattern that produces stretching along the axis between the upper left and lower right corners. If this transfer mechanism is important, then the feature shown in Figure 18(b) should have large (positive or negative) values on a smaller scale in the plane normal to the axis of stretching. This relationship needs to be studied in applications to observed and simulated flow fields. As just described, the method would be applied to two-dimensional features in two steps. It would be worthwhile looking at three-dimensional features, but to do so would be difficult. In the example just discussed, the features in Figure 18(a) will be of a smaller scale than those in Figure 18(b), and they will be oriented normal to the stretching axis.

Figure 19 shows an example of a three-dimensional vector feature that corresponds to vertical stretching of an eddy in the horizontal plane. In this case, the value assigned for the feature at the center point would be the sum of the scalar products of the feature vectors with the corresponding vector in the field being analyzed. Once the feature strengths have been determined for

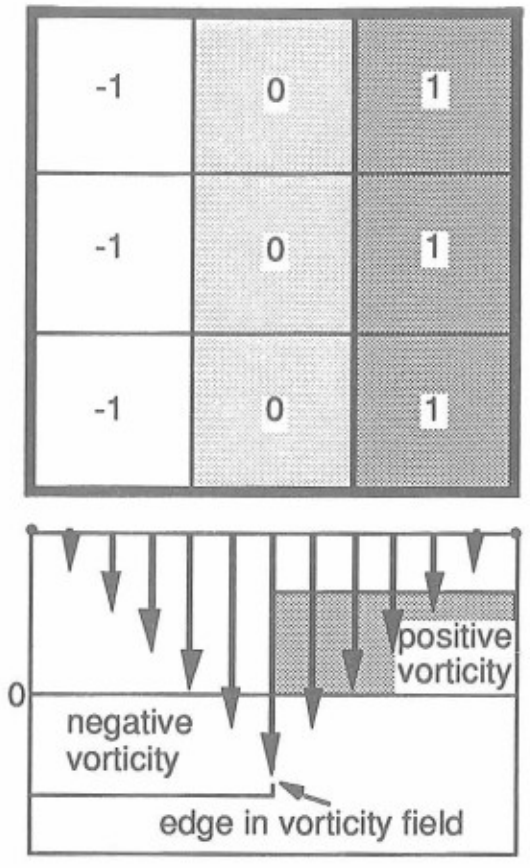

FIGURE 17 AN EDGE FEATURE AND A VELOCITY FIELD THAT PRODUCES AN EDGE IN THE VORTICITY FIELD

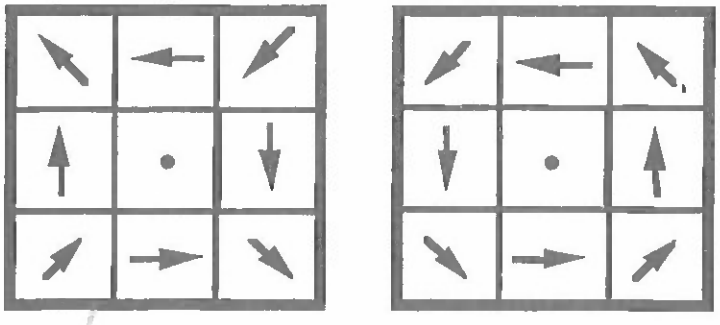

(a) (b)

FIGURE 18 TWO-DIMENSIONAL VECTOR FEATURES FOR TWO DIFFERENT TYPES OF SINGULARITY

(a) HYPERBOLIC POINT

(b) COUNTERCLOCKWISE VORTEX

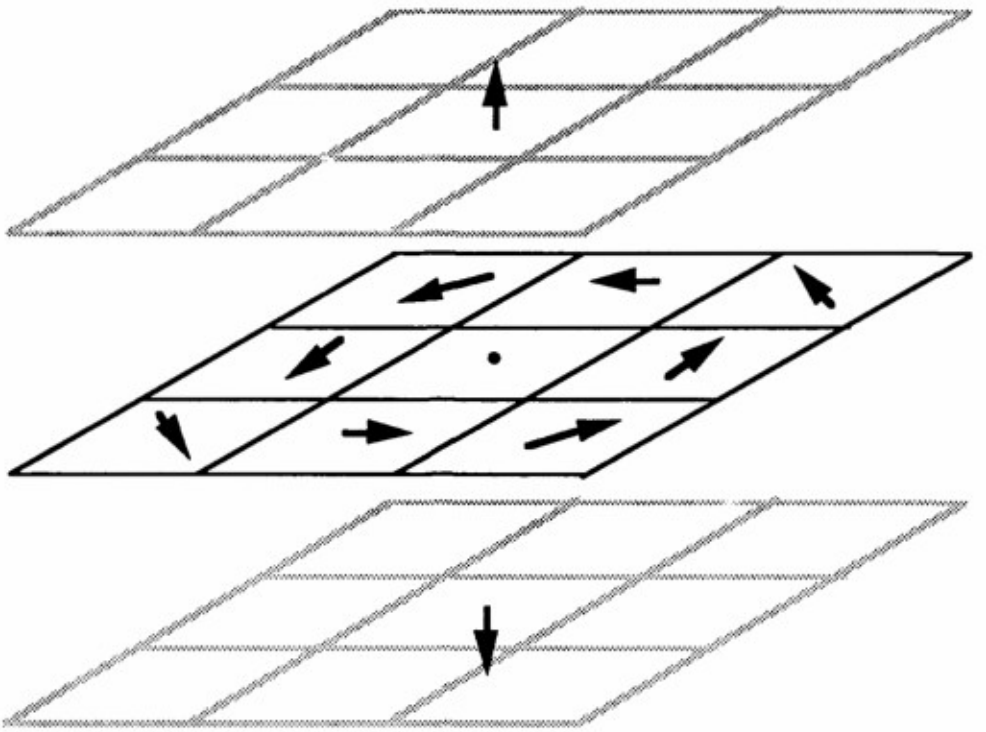

FIGURE 19 EXAMPLE OF A THREE-DIMENSIONAL VECTOR FEATURE

variously smoothed vector fields, the information necessary for multiresolution analysis is available. The dual Doppler radar wind data discussed earlier should provide a good basis for case studies. Although the number of data points in any one field may be too small, grouping the data should give sufficiently large samples for analysis.

2. Empirically Defined Features

One problem that arises in the use of vector features (and to a lesser extent, scalar features as well) is that one quickly runs out ideas for features. Furthermore, unless one is careful, there may be considerable redundancy of information among the members of any set of features that is arbitrarily defined (i.e., they may be linear combinations of one another). Thus, to carry this approach the logical next step, it would be desirable to have an approach to the definition of features that was based on the characteristics of the data themselves, and that provided features that were independent of one another. It would also be desirable to have a measure of the relative importance of the different features.

In the case of scalar features, an approach that is widely known is available. For example, Lorenz (1956) represented the patterns of variability of atmospheric pressure at 64 stations in the United States as a linear combination of independent patterns of variability, which he referred to as *Empirical Orthogonal Functions* (EOF). Lumley (1967, 1980) suggested that a similar kind of analysis could be used to extract coherent structures from turbulent flows. Ludwig and Byrd (1980) also applied the concept to vector fields. They identified patterns of variability in the

inputs used for a wind model in order to simplify the resulting calculations. Sirovich (1988) describes the analysis of turbulent flows by a similar procedure. According to Sirovich (personal communication, 1991), the patterns of variability can be identified without as much calculation as is required by the covariance matrix diagonalization approach described by Lorenz (1956), and adapted for use with vectors by Ludwig and Byrd (1980). The newer approach has not been tried yet.

The approach that has been pursued here uses small $3 \times 3 \times 3$ subsections of the observed wind field. Subtracting the center vector from each of the surrounding 26 vectors in the subsection gives a difference vector (Δv) for each of the points in the subsection, i.e.,

$$(\Delta \mathbf{V}_{ijk})_m = \begin{bmatrix} \Delta u_{ijk} \\ \Delta v_{ijk} \\ \Delta w_{ijk} \end{bmatrix}_m = \begin{bmatrix} u_{ijk} - u_{222} \\ v_{ijk} - v_{222} \\ w_{ijk} - w_{222} \end{bmatrix}_m , \tag{52}$$

where u_{ijk},v_{ijk} and w_{ijk} are vector components at point ijk (222 is at the center of the subsection) in the m^{th} subsection. The three-dimensional array of ΔVs shows the local pattern of motion about the center point. If we have this array and the vector $\mathbf{V}_{222}$ at the center point, then we can reconstruct the 26 surrounding vectors. Looking ahead to possible applications, we can envision that we have modeled the vectors on a coarse array (corresponding to the center point values). Then, if we have some way of estimating the array of ΔVs, we can obtain the field with finer resolution.

Next, we determine the deviations $\Delta \mathbf{V}'$ about the means by subtracting the average (indicated by the overbar) over the same relative points in all N subsections from individual $\Delta \mathbf{V}$'s, i.e.,:

$$\left(\Delta \mathbf{V}'_{ijk}\right)_m = \left(\Delta \mathbf{V}_{ijk}\right)_m - \overline{\left(\Delta \mathbf{V}_{ijk}\right)} . \tag{53}$$

This relative variability about the center point is described by ($3 \times 3 \times 3$ grid points) $\times$ 3 vector components. These 81 numbers are treated as the components of a column vector describing the "state" of the subsection. A matrix of these "state vectors" is multiplied by its transpose to give the covariance matrix for the complete set of state vectors. The eigenvectors of this matrix that account for the most variance in the individual patterns can be used as the "features" in the modified multiresolution feature analysis methodology. These eigenvectors are the empirical orthogonal functions (EOFs) that will be used for subsequent feature analysis.

The same approach can as easily be applied to scalar fields, differing only in that there is but one number associated with each grid point, so that it is computationally feasible to look at larger patterns of variability with scalars. Identification of the major patterns of variability in scalar

fields and how they scale with size could probably be used to guide smoke plume simulation methodologies like that recently described by Hoock (1991). He redistributes smoke material to smaller size elements based on the space-fillingness derived from an estimate of the fractal dimension. It is easy to see that the redistribution could be guided by the observed patterns of variability and their relative frequencies, rather than by purely random redistribution.

FORTRAN programs have been written to determine the most important features in three-dimensional vector arrays and two dimensional scalar arrays. The programs were applied to determine the vector features for the dual Doppler radar observations of winds near Boulder, Colorado for 1246 MST on 22 June 1984 (Schneider, 1991). The average variability about the center point of $3 \times 3 \times 3$ subsections of the wind field and the three vector EOFs that explain the most variance are shown in Figure 20. The strong shear in the wind field is evident in the average pattern of variability. The first EOF indicates a tendency for small-scale patterns (on the order of 400 m on a side) to show strengthening and weakening of vortex patterns tilted in the approximate direction of the shear. The second most important pattern of local spatial fluctuation (explaining almost as much variance as the first), is a general strengthening or weakening of the existing shear. The third EOF is somewhat more complex (and higher order EOFs tend to be even more so); its most important feature is that it accounts for local strengthening (and weakening) of the horizontal shear in approximately the north-south direction. The results of this application are encouraging. It is hoped that the techniques alluded to by Sirovich (1988) can reduce the required calculations. In any event, I expect to continue development and application of these techniques to atmospheric wind measurements.

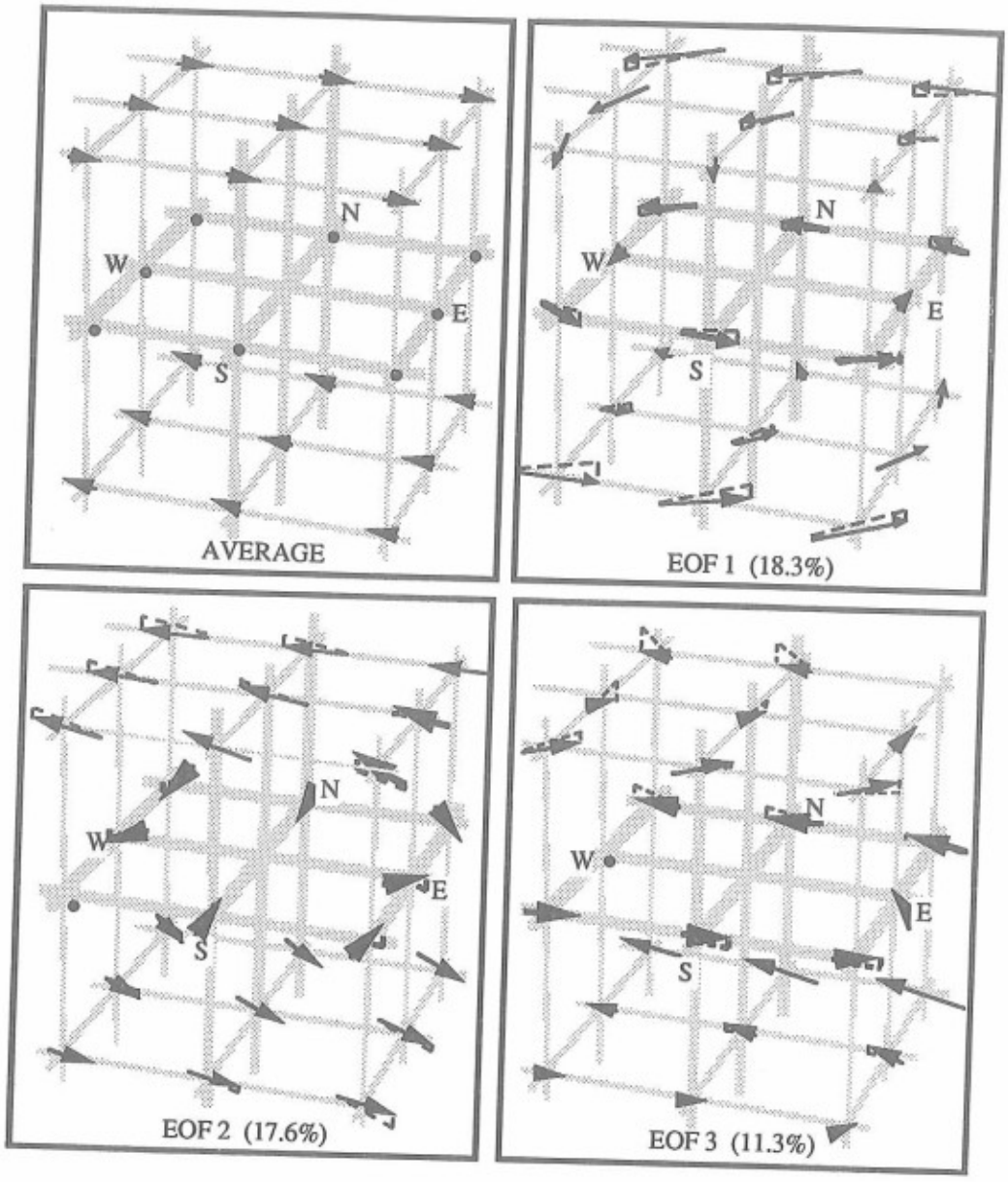

FIGURE 20 AVERAGE VARIATION ABOUT THE CENTER POINT AND THREE MOST IMPORTANT PATTERNS OF VARIATION IN AN OBSERVED WIND FIELD. (PERCENTAGE OF EXPLAINED VARIANCE IS SHOWN)

IV FUTURE RESEARCH

A. SUBGRID FLOW SIMULATION

1. Deterministic Approaches

It is quite possible that the EOFs will depend on the prevailing meteorology. For example, there is a tantalizing hint of this in the first EOF shown in Figure 20. Although it may just be happenstance that it has an axis that tilts from the vertical in the direction of the large-scale shear, it would not be surprising to find that the EOFs are affected by such things as the large-scale circulation, thermal stratification, and so forth. Furthermore, the most important EOFs may exhibit important changes from one level of resolution to the next. Such variability would complicate matters, but should not prevent the kinds of analyses discussed below from being performed.

It should somehow be possible to characterize the nature and strength of the most important features at a small scale from information available at coarser scales. If the field is fractal, then it should at least be possible to define the probability distribution of feature strengths, opening the way to probabilistic simulations of small-scale features. Of course, it will be easier if some reasonable correlations can be found between feature strengths at on scale and those at smaller resolutions. This would open the door to a simpler, more "deterministic" relationship between scales. There are two possibilities, but in either case the process begins by defining the several most important EOFs for a combined set of wind fields that correspond to similar meteorological conditions. The EOFs will be defined for each resolution and for the combined data set comprising of all the different smoothings. Then, either the EOFs for the combined resolutions closely resemble those derived for each of the smoothings, or they differ substantially from one another. In the first case, we choose one set of EOFs from those that have been calculated. Initially, this will probably be a subjective choice, but an objective selection scheme based on the inner products of the EOFs (which are actually large vectors) should not be difficult to devise. The next step is to use the most important EOFs as features and determine their strength at the grid points for each smoothing in each of the wind fields of the set. These feature strengths can then be used directly in the scheme adapted from Jones et al. (1991) to estimate fractal dimensions and determine whether different values are associated with different features. These same data also provide the information necessary for developing deterministic or probabilistic relationships as described later.

If the EOFs are substantially different for different resolutions, then we can still use the EOFs derived from the combined smoothings as a basis for estimating fractal dimensions. However, for estimating smaller-scale circulations, it will be better to calculate feature strengths for each smoothed field based on the EOFs that have been found to explain the most variance for that particular resolution. Again, this will lead to a set of feature values associated with each grid point in each of the smoothed fields, However, those feature strengths will refer to different

features at the different resolutions. This will not necessarily present a problem when we search for deterministic or probabilistic relationships between features at different scales, but it is likely to introduce some difficulties in practical applications.

One approach to the analysis would begin by calculating the linear correlations between the feature strength (for each of the most important small-scale features) at points on the smallest scale grid, and the feature values for the most important features at nearby points on the next coarser grid. There are some limitations on the choice of variables that are imposed by the geometry, i.e., the coarse grid points for which feature values can be calculated will all be farther removed from the edges of the domain than the finer scale points. Nevertheless , it is likely that we will end up with a correlation matrix of about 4 (important fine-scale features) $\times$ 108 (representing four features for each of the nearest 27 points). If the linear correlation table does not have any high correlations, it would probably be worthwhile to repeat the process using rank correlations in case there are significant monotonic, but nonlinear, relationships in the data.

If significant correlations are found, their distribution through the table may be very enlightening. For example, if the correlations are higher for feature values at more distant points than for the values at the central point, it suggests that the transfer of motion to smaller scales involves small-scale features "attached" to the larger features, rather than "embedded" in them. Correlations between different kinds of features could provide hints about the physical processes involved. For example correlation between small scale "eddy-like" features and larger-scale "stretching" features might be evident if the oft-suggested cascade via vortex stretching is important.

If some instances of high correlations are found, then those coarse features that are most highly correlated with the smaller-scale feature values would be used as input to an optimized multiparameter regression scheme to provide a functional relationship between the values of coarse-scale features and those of the most important smaller-scale ones. If the relationships were generally valid for all cases with similar meteorological conditions, then the regression results would provide all the required information for an extrapolation to smaller scales. The larger-scale feature intensities can be derived directly from the large-scale grid values, whether obtained by simulation or observation. Those feature values in turn are used to estimate the feature values for the next smaller scale, which serves as basis for estimating small-scale values from the center point value (which is at a coarse grid point), average variations about that point, and a linear combination of the features, using their estimated strengths as the coefficients.

2. Probabilistic Approaches

If there are no strong correlations between feature strengths at the smallest scale and those at the next largest, the problem is much more difficult, but there are at least two possible approaches that can be tried. Both are related to the probability of occurrence of feature strengths (or combinations of feature strengths) on the small scale to those on the larger scale. The fact that little or no correlation was found, combined with the presumed fractal nature of the fields, suggests the use the scaling properties to define the small-scale feature intensity probability distributions and use them in a Monte Carlo scheme to define a small-scale feature strength for each important feature around each coarse grid point. The orthogonality of the features

guarantees that their strengths are uncorrelated, so the probability distributions can be used independently without worrying about possible cross correlations. Once a feature strength has been defined for each feature type at each grid point, the process of constructing the smaller scale values proceeds just as described above for the deterministic case.

If no strong correlations are found between the strengths of individual feature types at the different scales, it would be worth exploring the possibility of using "clusters" of feature strengths to stratify the analysis. One of the standard cluster analysis programs would be used to identify groupings of feature strengths at the coarse and fine scales. Each coarse grid point would be identified with one of the coarse clusters and with one of the fine clusters. Then, contingency tables would be constructed to show the probability of occurrence for each fine-scale cluster, given the occurrence of a specified coarse cluster. These contingency tables could be used in a Monte Carlo scheme to select a fine-scale cluster for each grid point, given the coarse cluster that was appropriate to that point. We could calculate an average value for each feature strength, based on the members of the cluster, and use those feature strengths as described before to construct a local fine scale field. In essence, if this approach were applied to scalars, it would be a refinement of that described by Hoock (1991). He selects the smaller cells in which material is to appear randomly (with the average number of such cells defined by the fractal dimension), rather than by having preferred patterns of distribution.

With incomplete approximation (not all EOFs used), it is likely that the local vector (or other fields will violate various laws of physics—especially if full set of dynamic variables are included. Thus, it may be necessary to adjust the first-guess field to be compatible with governing equations. Possibilities include iterative relaxation schemes and variational calculus approach to get minimum adjustment.

B. FRACTAL/SCALING PROPERTIES

The multiresolution feature-analysis methodology requires the calculations of "feature strength" fields at all scales. These are scalar fields (regardless of whether the original field was scalar or vector) that can be used as input to any of the other fractal dimension calculation schemes, which would provide a link to other studies. It would also serve as another method for examining whether different aspects of the field are distributed in space with different scaling properties. This would not be surprising, as the different patterns represent different aspects of the flow (or scalar distribution). As an example, it was shown earlier that the vertical component of vorticity can be expressed as a vector feature. Its distribution might well be expected to be different from that of other scalars, such as speed, divergence, or other flow characteristics.

One interesting question that may need to be addressed is the following: Does the variance explained by the EOFs come from many common "events" of modest size, or from a few extreme cases? The former would be more useful for ordinary fluid flow parameterization applications. The latter would be more useful for addressing extreme value concerns, but it seems unlikely that it would be possible to acquire large enough data sets with the required wide range of scales.

REFERENCES

Barnsley, M.F. and A.D. Sloan, 1988: "A Better Way to Compress Images," *Byte* (January), pp. 215-223.

Bleiweiss, M., R. Howerton, R. Valdez, K. Payne, T. King and K. Hutchison, 1991: "A Comparison of the MPTR and ATLAS Transmissometers," *Proceedings of the Eleventh EOSAEL/TWI Conference*, Las Cruces New Mexico, U.S. Army Atmospheric Sciences Laboratory, White Sands Missile Range, New Mexico, pp. 605-612

Chorin, A.J., 1982: "The Evolution of a Turbulent Vortex," *Commun. Math. Phys.*, Vol. 83, pp. 517-535.

Feder, J., 1988: *Fractals*, Plenum Press, New York, 283 pp.

Frisch, U., P.-L. Sulem, and M. Nelkin, 1978: "A Simple Dynamical Model of Intermittent Fully Developed Turbulence," *J. Fluid Mech.*, Vol. 87, pp. 719-736.

Fujisaka, H. and H. Mori, 1979: "A Maximum Principle for Determining the Intermittency Exponent μ of Fully Developed Steady Turbulence," *Progress of Theoret. Phys.*, Vol. 62, pp. 54-60.

Gifford, F., Jr., 1957: "Relative Atmospheric Diffusion of Smoke Puffs," *J. Meteorol.*, Vol. 14, pp. 410-414.

Greenside, H. S., A. Wolf, J. Swift, and T. Pignataro, 1982: "Impracticality of a Box-Counting Algorithm for Calculating the Dimensionality of Strange Attractors," *Phys, Rev. A*, Vol. 25, pp. 3453-3456.

Hentschel, H.G.E. and I. Procaccia, 1983: "Fractal Nature of Turbulence as Manifested in Turbulent Diffusion," *Phys. Rev. A*, Vol. 27, pp. 1266-1269.

Hoock, D.L., 1991: "A Modeling Approach to Radiative Transfer through Inhomogeneous Dust and Smoke Clouds," *Proceedings 11th EOSAEL/TWI Conference*, U.S. Army Atmospheric Sciences Lab., White Sands Missile Range, New Mexico, pp 575-606.

Jones, J.G., R.W. Thomas and P.G. Earwicker, 1991: Multiresolution Analysis of Remotely Sensed Imagery, " *Internat. J. Remote Sensing*, Vol. 12, pp. 107-124.

Leonard, A., 1985: "Computing Three-Dimensional Incompressible Flows with Vortex Elements," *Ann. Rev. Fluid Mech.*, Vol. 17, pp. 523-559.

E.N. Lorenz, 1956: "Empirical Orthogonal Functions and Statistical Weather Prediction," Scientific Report 1, Statistical Forecasting Project, Massachusetts Institute of Technology, Cambridge, MA, Defense Document Center (DDC) No. 110268, 49 pp.

Lovejoy, S., 1982: "The Area-Perimeter Relation for Rain and Cloud Areas," *Science*, Vol. 216, pp. 185-187.

Lovejoy S. and D. Schertzer, 1986: "Scale Invariance, Symmetries, Fractals, and Stochastic Simulations of Atmospheric Phenomena," *Bull. Amer. Meteorol. Soc.*, Vol. 67, pp. 21-32.

Lovejoy, S., D. Schertzer and A.A. Tsonis, 1987: "Functional Box-Counting and Multiple Elliptical Dimensions in Rain," *Science*, Vol. 235, pp. 1036-1038.

Ludwig, F.L., 1989, "Atmospheric Fractals—A Review," *Environ. Software*, Vol. 4, pp. 9-16.

Ludwig, F.L. and G. Byrd, 1980: "A Very Efficient Method for Deriving Mass Consistent Flow Fields from Wind Observations in Rough Terrain," *Atmos. Environ.*, Vol. 14, pp. 585-587.

Lumley, J.L., 1967: "Coherent Structure in Turbulence," *Atmospheric Turbulence and Radio Wave Propagation* (edited by A.M. Yaglom and dV I. Tatarski), Nauka, Moscow, pp. 166-178. (Referenced by Sirovich, 1988).

Lumley, J.L., 1980: "Coherent Structures in Turbulence," Transition and Turbulence (edited by R. E. Meyer), Academic Press, New York, pp 215-241.

Mandelbrot, B.B., 1975: "On the Geometry of Homogeneous Turbulence, with Stress on the Fractal Dimension of the Iso-Surfaces of Scalars," *J. Fluid Mech.*, Vol. 72, pp. 401-416.

Mandelbrot, B.B., 1977: "Intermittent Turbulence and Fractal Dimension: Kurtosis and The Spectral Exponent 5/3+B," *Lecture Notes in Mathematics (565), Turbulence and Navier-Stokes Equations*, (ed. R. Temam) Springer-Verlag, Berlin, pp. 121-145.

Mandelbrot, B.B., 1983: *The Fractal Geometry of Nature*, W. H. Freeman and Co., NY, 468 pp.

Mandelbrot, B.B., 1985: "Self-Affine Fractals and Fractal Dimension," *Physica Scripta*, Vol. 32, pp. 257-260.

Pentland, A.P., 1984: "Fractal-Based Description of Natural Scenes," *IEEE Trans. Pattern Anal. and Machine Intelligence, PAMI-6*, pp. 661-674.

Prasad, R.R. and Sreenivasan, K.R., 1990: "Quantitative Three-Dimensional Imaging and the Structure of Passive Scalar Fields in Fully Turbulent Flows," *J. Fluid Mech.*, Vol. 216, pp. 1-34.

Press, W.H., B P. Flannery, S.A. Teukolsky and W. T. Vettering, 1988: *Numerical Recipes*, Cambridge University Press, Cambridge, 818 pp.

Procaccia, I., 1984: "Fractal Structures in Turbulence," *J. Stat. Phys.*, Vol. 36, pp. 649-663.

Reynolds, W.C., 1985: Class notes for Mechanical Engineering 261B, "Turbulence Modeling," Stanford University, Stanford, California.

Richardson, L.F., 1922: *Weather Prediction by Numerical Process*, Cambridge University Press. (Cited by Mandelbrot, 1983)

Richardson, L.F., 1926: "Atmospheric Diffusion Shown as a Distance-Neighbor Graph," *Proc. Roy. Soc. London, Series A, 110*, 709-737.

Rys, F.S. and A. Waldvogel, 1986: "Fractal Shape of Hail Clouds," *Phys. Rev. Let.*, Vol. 56, pp. 784-787.

Saupe, D., 1988: "Algorithms for Random Fractals," *The Science of Fractal Images*, (H-O Peitgen and D. Saupe, eds.), Springer-Verlag, New York, pp. 71-136.

Schertzer, D. and S. Lovejoy, 1983: "The Dimension and Intermittency of Atmospheric Dynamics," *Turbulent Shear Flows 4*, (L. J. S. Bradbury et al., editors) Springer Verlag, Berlin, pp. 7-33.

Schertzer, D. and S. Lovejoy, 1987: "Physical Modeling and Analysis of Rain and Clouds by Anisotropic Scaling Multiplicative Processes," *J. Geophys. Res.*, Vol. 92(D8), pp. 9693-9714.

Schneider, J.M., 1991: *Dual Doppler Measurement of a Sheared, Convective Boundary Layer*, PhD dissertation, U. of Oklahoma, Norman, Oklahoma, 133 pp.

Sirovich,L., 1988: "Analysis of Turbulent Flows by Means of the Empirical Eigenfunctions," Brown University, Center for Fluid Mechanics Report No. 90-212, 40 pp.

Takens, F., 1981: "Detecting Strange Attractors in Turbulence," *Dynamical Systems and Turbulence*, (ed. D.A. Rand and L.A. Young), Springer Verlag, Berlin, 366-381.

Uthe, E.E., 1983: "Application of ALPHA-1 Plume Model Validation and Development—Plains Site," Final Report SRI International Project 1616, Electric Power Research Institute Report EA-3073, Palo Alto, California, 62 pp.

Van Dyke, M., 1982: *An Album of Fluid Motion*, Parabolic Press, Stanford, California, 176 pp.

Voss, R.F., 1988: "Fractals in Nature: From Characterization to Simulation," *The Science of Fractal Images*, (H-O Peitgen and D. Saupe, eds.), Springer-Verlag, New York, pp. 21-70.

Appendix A

PRESENTATIONS AND PUBLICATIONS RELATING TO WORK PERFORMED ON THE PROJECT

CONFERENCE PRESENTATIONS

Ludwig, F.L. "A Review of the Application of Fractals to the Representation of Atmospheric Processes," Eighth EOSAEL/TWI Conference, Las Cruces, New Mexico, December 1-3, 1987.

Ludwig, F.L., "Analysis of Lidar Cross Sections of Smoke Plume Cross Sections," Conference on Nonlinear Variability in Geophysics, Paris, France, June 27-July 1, 1988.

Ludwig, F.L., "Use of Fractal Concepts in the Analysis of Atmospheric Inhomogeneities," 17th NATO/CCMS International Technical Meeting on Air Pollution Modeling and Its Application," Cambridge, U.K., September 19-22, 1988.

Ludwig, F.L., "Atmospheric Fractals—A Review," Evirosoft 88 Conference, Porto Carras, Greece, September 27-29, 1988.

Ludwig, F.L., "Using Multi-Resolution Feature Analysis To Interpret Atmospheric Observations," Eleventh Annual EOSAEL/TWI Conference, Las Cruces, New Mexico, November 27-30, 1990.

Ludwig, F.L., "Multi-Resolution Feature Analysis of Atmospheric Motion Using Empirically Defined Features," Dynamic Days Workshop, Berlin, June 12-15, 1991.

Ludwig, F.L., "Empirically Defined Structures in a Sheared Convective Atmospheric Boundary Layer," submitted to Fall 1991 meeting of The American Geophysical Union, San Francisco, December 9-13, 1991.

PUBLISHED PAPERS

Ludwig, F.L., 1988: "A Review of the Application of Fractals to the Representation of Atmospheric Processes," *Proc. 8th EOSAEL/TWI Conference* U.S. Army Atmospheric Sciences Lab., White Sands Missile Range, New Mexico, pp. 401-410.

Ludwig, F.L., 1988: "Atmospheric Fractals—A Review," *Computer Techniques in Environmental Studies* (Computational Mechanics Pubs., Southhampton, UK, and Springer-Verlag, Berlin), pp. 333-357.

Ludwig, F.L., 1989: "Atmospheric Fractals—A Review," *Environmental Software,* Vol. 4, pp. 9-16.

Ludwig, F.L., 1989: "Fractal Concepts and The Analysis of Atmospheric Inhomogenieties," *Air Pollution Modeling and Its Application*—VII (Plenum Press, New York), pp. 451-460.

Ludwig, F.L., 1991: "Using Multi-Resolution Feature Analysis to Interpret Atmospheric Observations," *Proceedings 11th EOSAEL/TWI Conference*, U.S. Army Atmospheric Sciences Lab., White Sands Missile Range, New Mexico, pp. 623-631.

Appendix B

PARTICIPATING SCIENTIFIC PERSONNEL

Francis Ludwig, Principal Scientist

Murray Baron, Director, Geosciences and Engineering Center

John Herndon, Principal Computer Applications Analyst

Jean Jacobson, Senior Technical Writer/Editor

John Perry, Senior Computer Applications Analyst

Raymond Trent, Software Engineer

Edward Uthe, Director Atmospheric Science and Effects Program

Appendix C

INVENTIONS

There were no inventions on this project.